공학박사학위논문

Electrokinetics of All-around-Gated Ambipolar Ionic Field Effect Transistor

All around gate를 이용한 전기장 구동 양극성 이온 트랜지스터의 electrokinetic 현상

2016년 2월

서울대학교 대학원

재료공학부

이 승 현

Electrokinetics of All-around-Gated Ambipolar Ionic Field Effect Transistor

All around gate를 이용한 전기장 구동 양극성 이온 트랜지스터의 electrokinetic 현상

지도 교수 김기범

이 논문을 공학박사 학위 논문으로 제출함

2016 2 월

서울대학교 대학원

재료공학부

이승현

이승현의 공학박사 학위 논문을 인준함

2016 년 2 월

위원장	남 기 태	(인)
부위원장	김 기 범	(인)
위 원	김 성 재	(인)
위 원	한 창 수	(인)
위 원	김 준 호	(인)

Electrokinetics of All-around-Gated Ambipolar Ionic Field Effect Transistor

All around gate를 이용한 전기장 구동 양극성 이온 트랜지스터의 electrokinetic 현상

A DISSERTATION SUBMITTED TO

DEPARTMENT OF MATERIALS SCIENCE AND ENGINEERING

SEOUL NATIONAL UNIVERSITY

FOR THE DEGREE OF

DOCTOR OF PHILOSOPHY

Seung-Hyun Lee

February 2016

Abstract

In this dissertation, the advanced device was developed for overcoming the limitation of IFET which can be manipulate charged species pass through nanochannel. And the slow response time of nanofuidic device was studied for improving the device.

we developed a versatile ionic field effect transistor (IFET) which has an ambipolar function for manipulating molecules regardless of their polarity and can be operated at wide range of electrolytic concentrations (10^{-5}M~1M). The IFET has circular nanochannels completely covered by gate electrodes, called "*all-around-gate*", with a aluminum oxide (Al_2O_3) of a near-zero surface charged oxide layer. Experimental and numerical validations were conducted for characterizing the IFET. We found that the versatility is originated from the zero-charge density of oxide layer and all-around-gate structure which increase the efficiency of gate effect 5 times higher than a previously developed planar-gate by capacitance calculations. Our numerical model adapts Poisson-Nernst-Plank-Stokes (PNPS) formulations with additional nonlinear constraints of fringing field effect and counter-ion condensation and the experiment and numerical results are well matched. The device can control the transportation of ions at severe concentration up to 1M electrolyte which resembles a backflow of a shale gas extraction process. Furthermore, while traditional IFETs can manipulate either

positively or negatively charged species depending on the inherently large surface charge of oxide layer, the presenting device and mechanism provide effective means to control the motion of both negatively and positively charged molecules which is important in DNA sequencing through nanopore, medical diagnosis system and point-of-care system, etc.

However the ambipolar IFET showed slow response time during ionic current measurement. Smeets analyzed the slow response time using a simple RC electric circuit, but it does not fit well to experiment data below t = 50 us. We hypothesized that the long response time comes from the electric double layer capacitor. Thus we developed a new model and equation that includes "EDL capacitor". Silicon nitride nanopore device was made by traditional fabrication method. The device measurement was done by patch clamp. By matching the new model to experimental data, we showed the possibility of a better theory than Smeets' equation.

Key words: nanofluidic, nanochannel, ionic field effect transistor, ambipolar behavior, response time, RC delay time

Student number: 2011-30786

Table of contents

List figures and tables

Chapter 1

Chapter 2

Chapter 3

Chapter 4

Chapter 5

Fig 5.8 Threshold voltages of various IFET devices. Thick planar gate on SiO_2 (□) and thin planar gate on SiO_2 (△) were referred from literatures

Chapter 6.

CHAPTER1. Nanofluidics: Introduction

1. 1 Nanofluidics

Nanofluidics is the study of behavior, manipulation, and control of fluids that are confined to structures of nanometer (below 100 nm) characteristic dimenstions.[1] Practical research of Nanofluidics began from 1990s because of the difficulty of following the nanofabrication below 100 nm. Despite the recently started, this study dramatically grew a large disciplines which currently published 1600 or more articles (Fig 1.1). The reason for this nanofluidics was able to develop a large disciplines, because the influence of electric double layer has been expanded depending on the move from micro size to nano size.

1.2 The influence of Electric double layer

Electric double layer is a native potential which is made from counter ion condensation for compensating with the surface charge of material in solution (Fig 1.2 (a)) [2]. Classically, this length of electric double layer is called Debye screening length and we will express the equation (1.1).

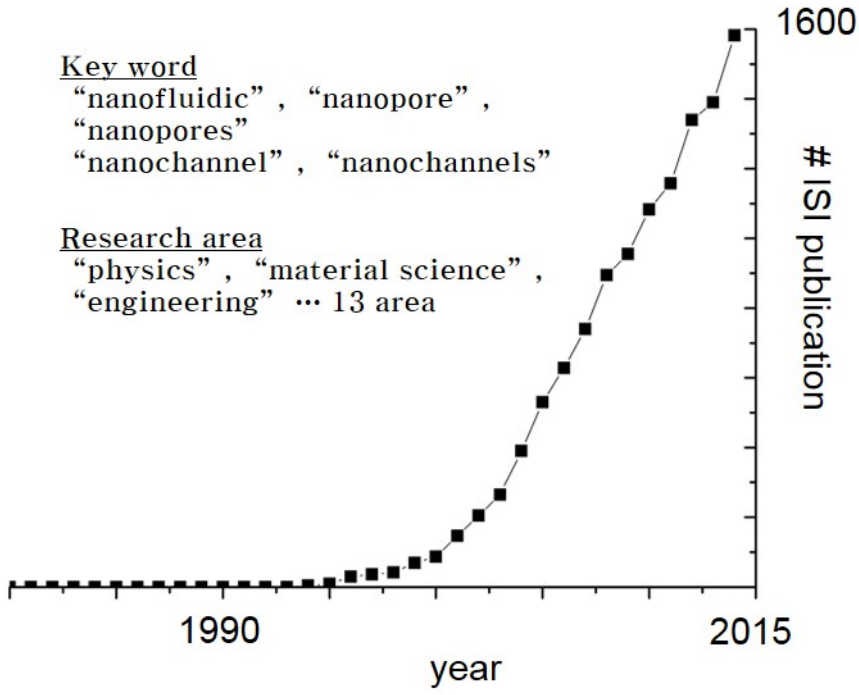

Fig 1.1 The number of ISI publications relating to the year. We used key wordword "nanofluidic", "nanopore", "nanopores" "nanochannel", "nanochannels". We searched area "physics", "material science", "engineering" and 13 area.

$$\lambda = \sqrt{\frac{k_B T \varepsilon_0 \varepsilon_r}{2z^2 e^2 n^\infty}} \qquad \text{Eq. (1.1)}^{3}$$

$n^\infty$is the concentration of bulk solution. Z is the ionic valence of solution. $\varepsilon_0, \varepsilon_r$ are respectively the permittivity of space and solution. The Debye screening length is changed as the concentration of standard solution from few angstrom to few hundred nanometer (Table 1.1)[3]. Therefore typical microfluidics which have few micro size or macro size can be ignore the influence of electric double layer (Fig 1.2(b)) [4]. As the wall approaches below nanoscale, new potential distribution is made by overlapping between the electric double layers of each wall (Fig 1.2 (c)) [4.] This new potential distribution show unique property of nanofluidics.

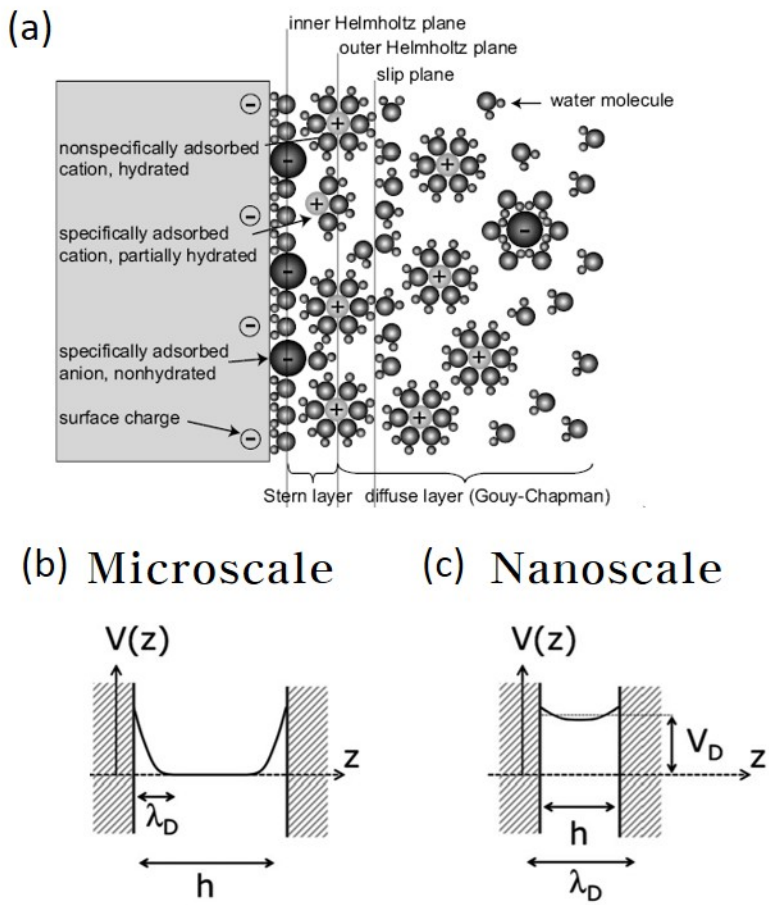

Fig 1.2 (a) the schematic figure of electric double layer. The potential distribution of (b) microscle, (c) nanoslcle.

1.3 Perm-selectivity

Perm-selectivity is one of important property from nanofluidics. This property is a term used to define the preferential permeation of certain ionic species through ion exchange membrane. [5] In nanofluidics, counter ion of material surface charge are filled inside nanochannel as overlapping the electric double layer. This phenomena makes it difficult that co ion pass through the nanochannel. As result, this nanochannel have a perm-selectivity (Fig 1.3 (a)). If we control the surface charge, co ion is more easily pass through nanochannel. Even through major carrier is opposite ion as changing opposite surface charge of material (Fig 1.3 (b)).

1.4 Application of Perm-selectivity

There are three application using the perm-selectivity. First application is applied to a water purification or desalination extracting a specific ion in nanochannel (Fig 1.4 (a)) [6].

Second is a clean energy application using the conversion of a mechanical pressure to an electrical flow which pass through specific charge ion in nanochannel (Fig 1.4(b)) [7]. Third application is bio application. Fig 1.4 (c) [8] show that we can manipulate to a

Table 1.1 Dye screening length with variation of KCL concentration

KCl concentration (M)	Debye length λ_D (nm)
10^0	0.3
10^{-1}	1.0
10^{-2}	3.1
10^{-3}	9.6
10^{-4}	30.5
10^{-5}	96.3

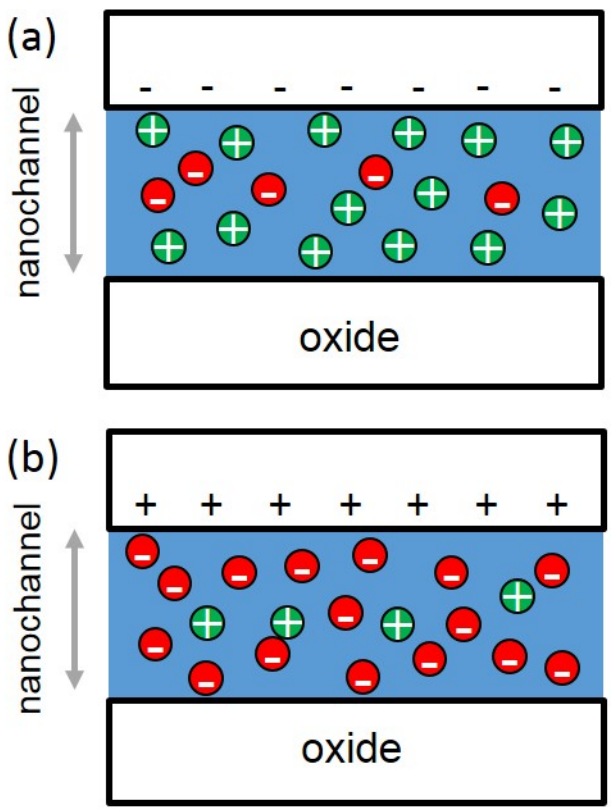

Fig 1.3 the permselectivity property of nanofluidics with (a)negative surface charge (b) negative surface chrage

velocity and direction of biomaterial through the nanochannel. This application gave us the possibility of a high resolution analysis.

The common points of these three applications is that the property of electric double layer is most important role of these devices and if it is able to regulate the electric double layer, thereby we produce a maximum efficiency of each device.

In this thesis, we answered two questions. First, how can electric double layer be modulated to enhance efficiency of nanofluidic device? We answered using the ionic field effect transistor. Second, how does electric double layer affect response time of nanofluidic device? We answered using the electric double layer capacitor.

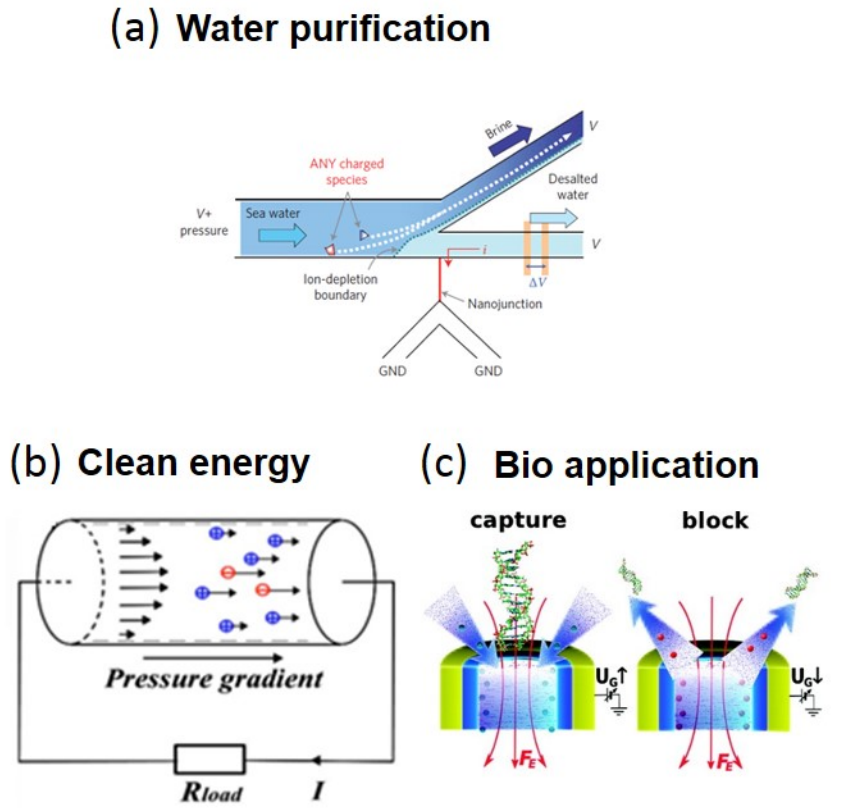

Fig 1.4 the application of nanofluidics (a)water purification (b)clean energy (c) bio application

Reference

(1) Wikipedia, https://en.wikipedia.org/wiki/Nanofluidics

(2) Z. Jiang; D. Stein, Langmuir, 26, 8161 (2010)

(3) Reto B. Schoch, Rev. Mod. Phys., 80, 839 (2009)

(4) Bocquet et al., Chem. Sov. Rev., 39, 1073 (2010)

(5) 세화 편집부, 화학대사전

(6) S. J. Kim et al., Nature Nanotech., 5, 297(2010)

(7) Y. B. Xie et al., Appl. Phys. Lett., 93, 163116(2008)

(8) Yuhui He et al., *ACS Nano*, 5, 8391 (2011)

CHAPTER2. The study of alternative material for the ambipolar IFET

2.1 Introduction

Various passive type of modulating the motion of a charged species in nanofluidic system were reported such as changing the viscosity of solution in the nanochannel[1] (Fig 2.1 (a)), mechanical friction between DNA and nanopore[2] (Fig 2.1 (b)), coating an adhesive material on nanochannel[3] (Fig 2.1 (c))and surface treatment for changing the surface potential[4] (Fig 2.1 (d)). Those platforms employed passive methods which were unable to change the behavior of charged species on-demand, once the devices were fabricated. In contrast, ionic field effect transistor (IFET) can provide an active method which enable to enhance, diminish or even reverse the behavior of charged species *in situ* by introducing gate potential.

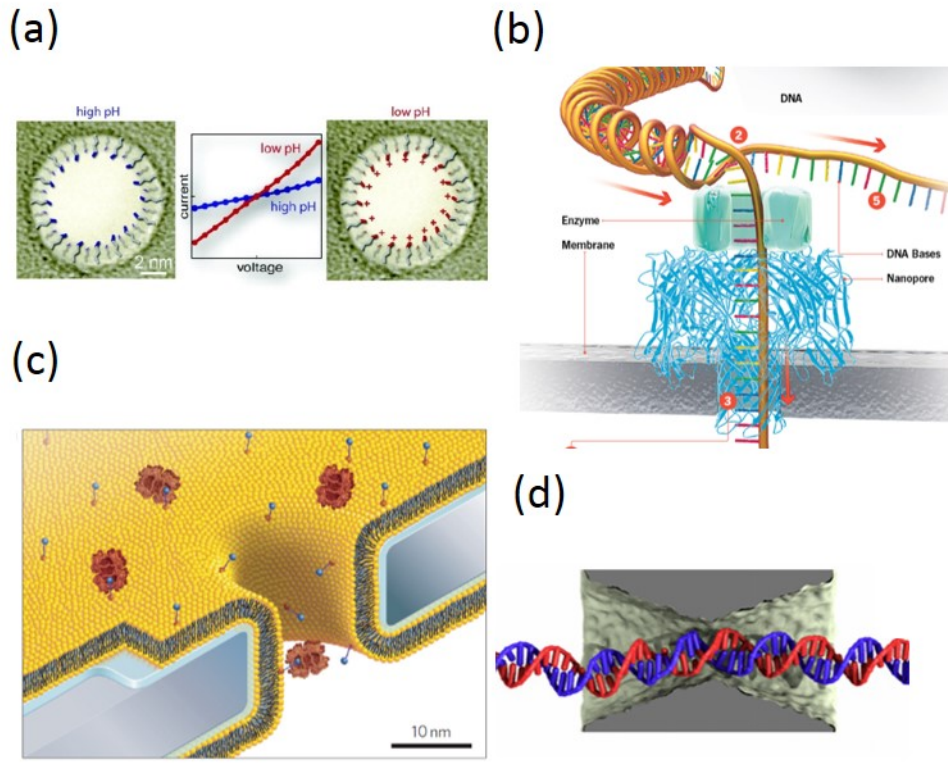

Fig 2.1 various passive method of modulating the motion of a charged spicies in nanofluidic system (a) changing a pH of solution (b) reformation of spices (c) coating an organic material (d) mechanical friction

2.1.1 Previous research limitation: Unipolar characteristics of IFET

Previous research were published various nanofabrication methods and device designs for ionic field effect transistor. Rong Fan made the 2 dimensional nanoslits which have micro size width and nano size height using reactive ion etching (RIE) and anodic bonding. (Fig 2.2(a)) [5] Udi vermesh made 1dimensional nanochannel using the sacrifice methods. This methods used wet etching for specific nanowire after depositing the oxide on the nanowire. (Fig 2.2 (b)) [6] Nam sung wuk made 0 dimensional nanopore using the electron beam llithography and RIE. (Fig 2.2 (c)) [7]

Even though various devices were fabricated, they have the same trend of experiment data and limitations due to use same concept.

Fig 2.3 (a) ~(c)[7,8,9] show that ionic current of all devices decreased as changing from negative gate voltage to positive gate voltage. The devices (Fig 2.3 (b), (c)) which have good gate efficiency show the saturation ionic current at positive gate voltage. When these trend analyze using the ionic conductance equation (Eq. (2.4)), surface charge were unable to change in the positive gate voltage because of their large surface charge.

Traditional IFETs can manipulate either positively or negatively charged species depending on the inherently large surface charge of oxide layer and they demanded either high gate voltage or low electrolyte concentration for changing surface charge density [5, 6, 7-

[11]. Traditional fabrication method of IFET was principally made by SiO_2 [5, 6, 8, 10, 11] and nanoporous membrane[9]. While they had transparency, easy-fabrication and relatively high uniformity, these materials had high surface charge density which led to a diode behavior[5, 6, 7-1111-16]. The reason why the diode behavior occurs is that induced surface potential by gate voltage cannot overcome a polarity of inherent surface potential. Due to this characteristic, a traditional IFET can only control the same polarity of charged species with the surface charge of nanochannel.

To overcome the limitation, we need to choose a new oxide material. Alternative material selection criteria are next tree condition. First, low leakage current like the SiO_2. Second, neutral surface charge for ambipolar behavior. Third, high dielectric constant for high gate efficiency.

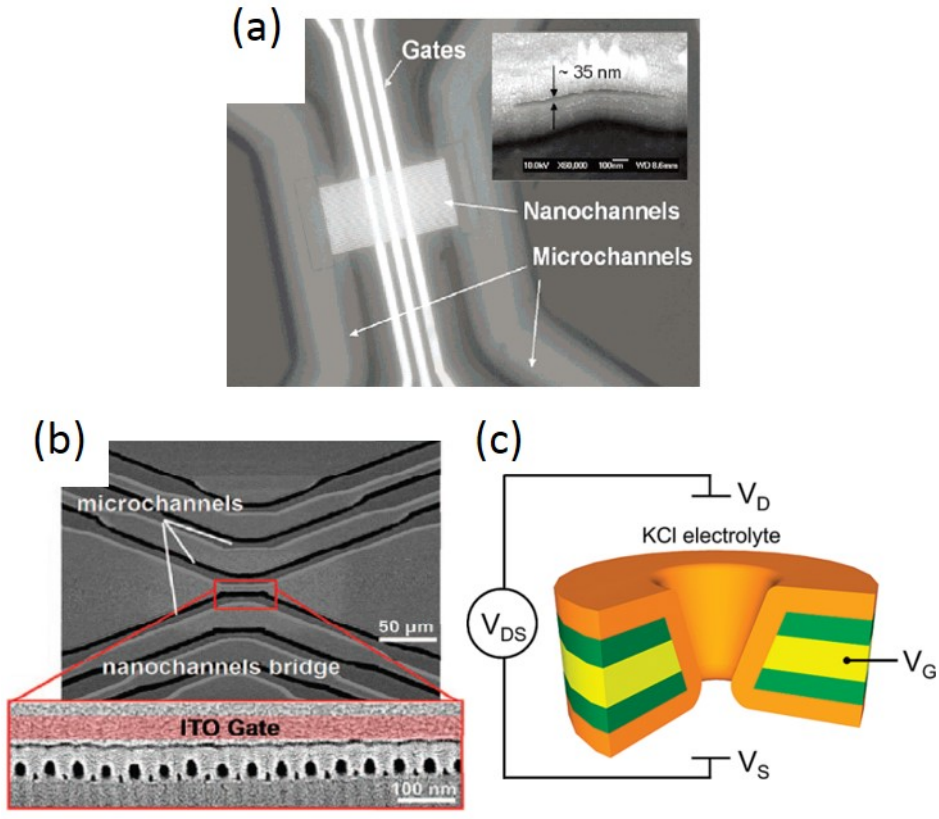

Fig 2.2 Design of IFETs as following fabrication methods.
(a) nanoslits 2D (b) nanochannel 1D (c) nanopore 0D

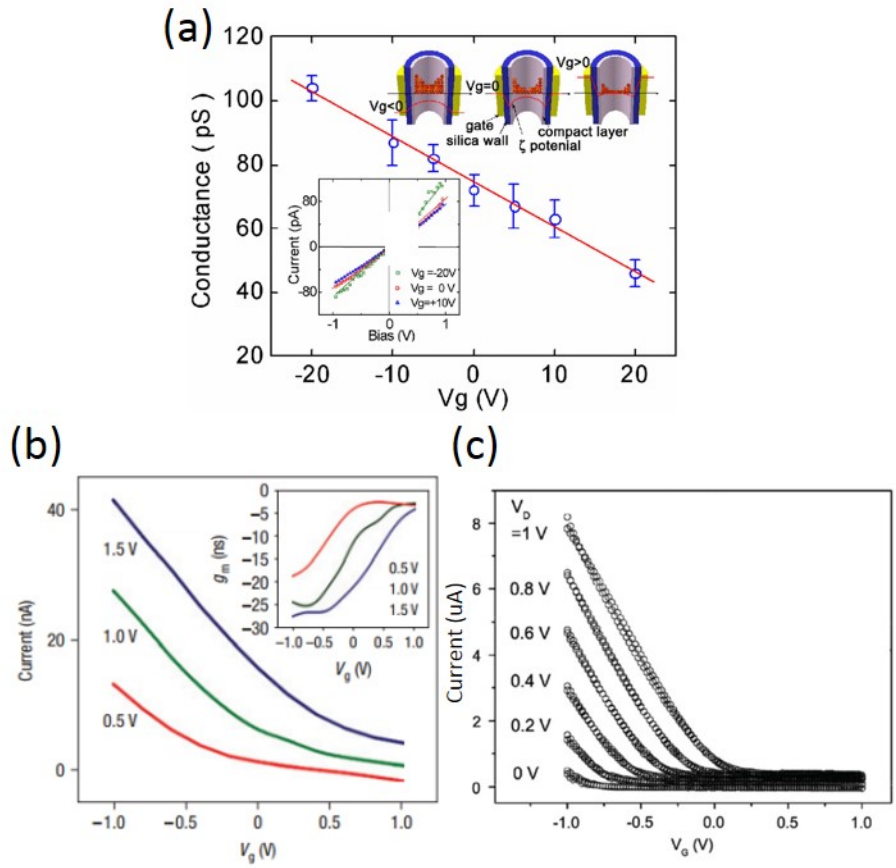

Fig 2.3 Ionic current – gate voltage graphs (a) nanoslits 2D (b) nanochannel 1D (c) nanopore 0D

2.2 Materials and methods

2.2.1 Literature research for alternative material selection

We examined literature value of the point of zero charge (PZC) (Fig 2.4 (a)) [11] and the dielectric constant (Fig 2.4 (b)) [12] for neutral surface charge and high-k constant. First, we chose four oxide ZrO_2, TiO_2, Si_3N_4 and Al_2O_3 using the PZC graph which displayed the pH value at the range of zero surface charge. Second, Si_3N_4 which have low dielectric constant like a SiO_2 was excluded for high gate efficiency. Finally, we have selected TiO_2 and Al_2O_3 which are enable to deposition using the atomic layer deposition (ALD) in our lab.

The surface charge of nanochannel played a deterministic role for the direction of ion transportation. In this work, we covered the nanochannel surface with aluminum oxide (Al_2O_3) as a dielectric layer. While the surface charge of Al_2O_3 is usually known to be (slightly) positive, our system had a slightly negative surface change due to its lower point-of-zero-charge than 7. To confirm the polarity, we had conducted ion concentration polarization (ICP) experiment that possessed an ion depletion zone at anodic side and

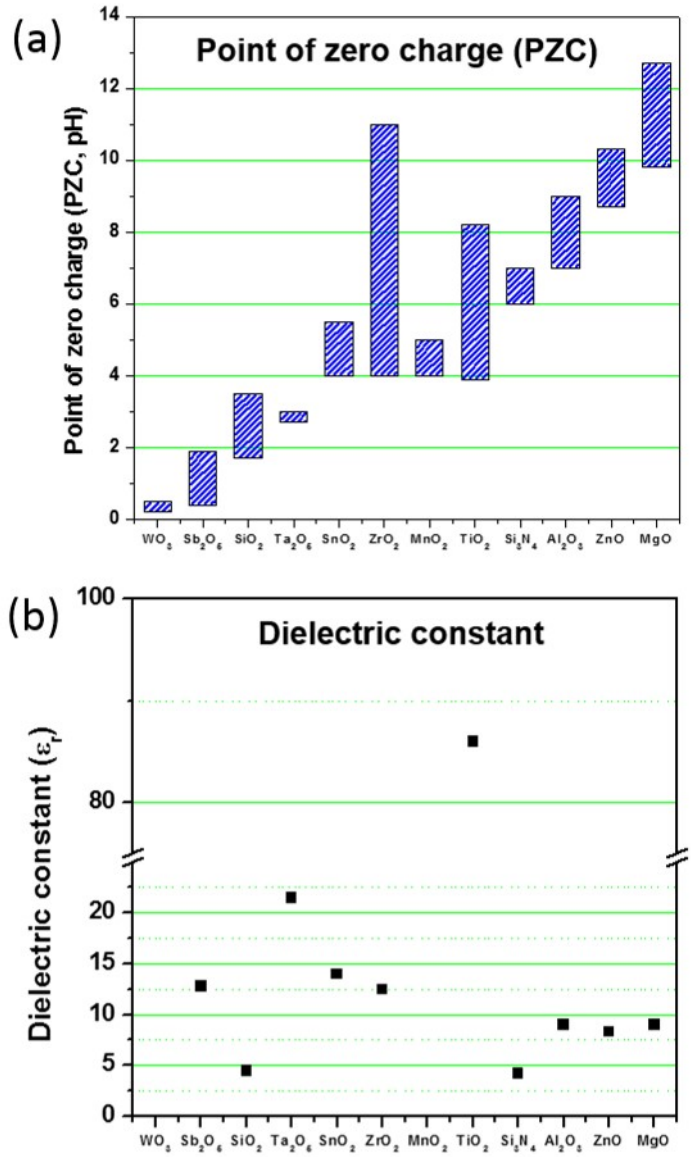

Fig 2.4 Literature research (a) point of zero charge (b) Dielectric constant

an ion enrichment zone at cathodic side with negatively charged nanochannels[40].

As shown in Figure 2.5, the fluorescent signal quickly disappeared at anodic side of nanochannel array to confirm that the ion depletion zone was formed at the anodic side. (Also see supporting video.) The ion depletion zone should be formed at the cathodic side if the surface charge of nanochannel was positive[41].

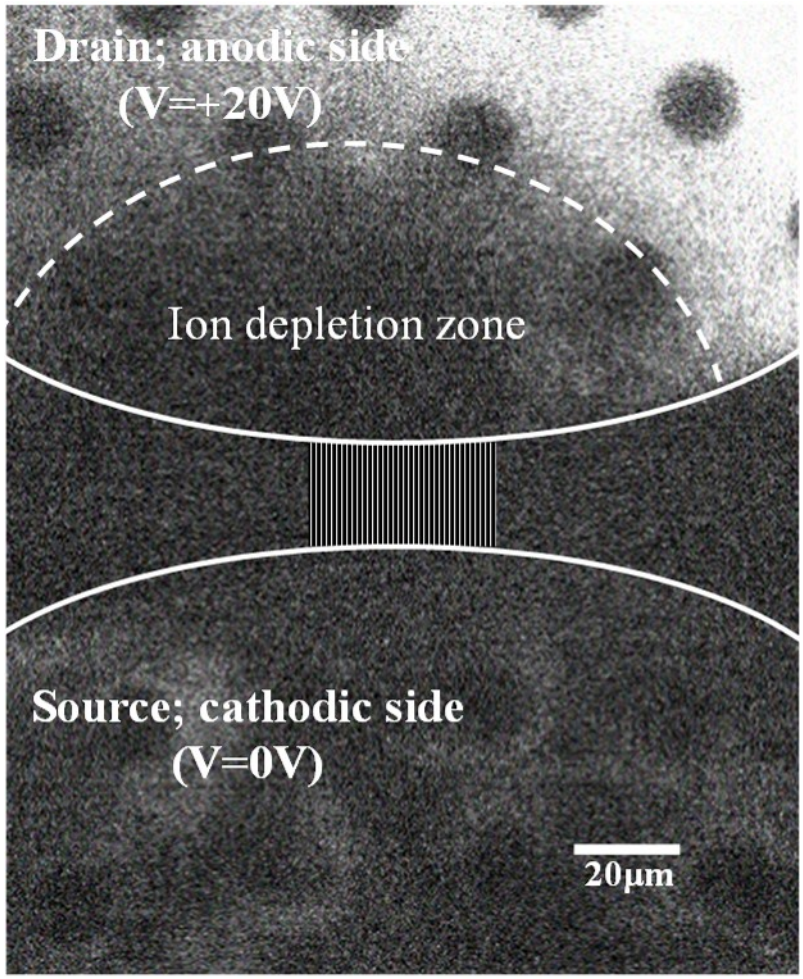

Fig 2.5 The formation of the ion depletion zone at the anodic side. This confirmed that Al_2O_3 surface was negatively charged.

2.2.2 Leakage current experiment of metal-oxide-electrolyte (MOE) system

The leakage current is the one of important parameter that affects the performance of device which have a gate structure. Therefore, it is important to recognize by simple experimentation how many leakage current flow through a gate oxide. In order to recognize the leakage current in the solution, we applied the Metal-Oxide-Electrolyte (MOE) system (Fig 2.6 (a)) instead of Metal-Oxide-Semiconductor (MOS) system in typical solid state. MOE device was fabricated by photolithography and reactive ion etching. Metal was deposited an aluminum using an evaporator. $TiO_2$and Al_2O_3 were deposited 60nm by ALD. Chamber of electrolyte was formed by SU-8 which is a photolithography resist and have a high hydrophobicity and a strong strength enough a function of chamber.

This MOE system which mimic the gate structure of IFET device can be able to check the leakage current before the device are fabricated. The leakage current of $TiO_2$and Al_2O_3 was measured by the MOE system. Fig 2.6 (b) was shown that Al_2O_3 have a lower leakage current than TiO_2. As result, the nanochannel were fabricated by Al_2O_3 which have a low leakage current, neutral surface charge density and high dielectric constant.

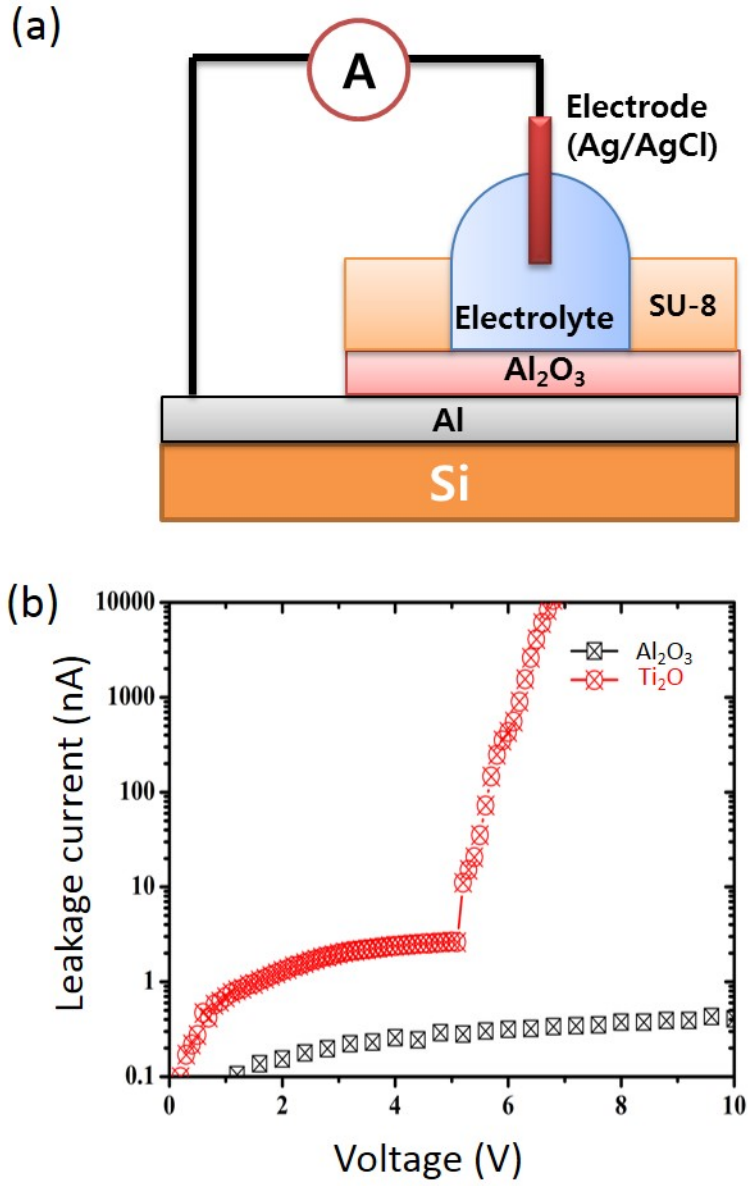

Fig 2.6 Metal oxide electrolyte system (MOE) (a) the schematic figure of MOE system. (b) the experimental data of leakage current using MOE system. We used Al_2O_3 and Ti_2O.

2.3 Results and discussion

2.3.1 Principle of ionic field effect transistor (IFET)

Ionic field effect transistor (IFET) can be able to control the perm-selectivity. The oxide surface which wrapped the nanochannel are affected by gate potential. Thereby the induced dielectric polarization add the native oxide surface charge. Then we can chose the polarity of surface charge by modulate the degree of gate potential. (Fig 2.7)

Ionic conduction in nanofluidics can be divided into two ionic conduction. (Fig 2.8) The equation (2.1) is the simple electric conduction equation. However we need to consider the more complex situation.

$$G = \frac{I}{V} = \frac{nq\mu E}{V} \qquad \text{Eq. (2.1)}$$

q is the elementary of charge [C], μ is electric mobility. First ionic conduction is considered geometry and bulk concentration and expressed using below equation (2.2)[7] this conduction is called “bulk concentration governed ionic conduction”.

$$G_{bulk} = \frac{\pi r_{nano}^2}{L_{nano}}[e \times n_{KCl}(\mu_{co} + \mu_{counter})] \qquad \text{Eq. (2.2)}$$

μ_{co} is the electrophoretic mobility of co ion, $\mu_{counter}$ is the electrophoretic mobility of counter ion, r_{nano} is the diameter of nanochannel and L_{nano} is the length of nanochannel. Second ionic conduction is considered geometry and counter ion in the electric double layer. The counter ion which is induced by surface charge of material additionally generate the "surface charge governed ionic conduction" and is expressed by below the equation (2.3)

$$G_{surf} = \frac{2\pi r_{nano}}{L_{nano}} [\mu_{counter} \times |\sigma_0|] \quad \text{Eq. (2.3)}$$

σ_0 is the surface charge density of oxide. These two ionic conduction have taken effect in the same nanochannel. Therefore we can directly add each other. And then we got the final ionic conductance the equation (2.4) in nanochannel.

$$G_{tot} = \frac{\pi r_{nano}^2}{L_{nano}} \left[(\mu_{co} + \mu_{counter}) n_{KCl} \times e + \mu_{counter} \frac{2|\sigma_0|}{r_{nano}} \right] \quad \text{Eq. (2.4)}$$

This equation (2.4) are divided the term which is determined by bulk solution and other term which is determined by surface charge. Surface charge is native property of material so ionic conductance of the passive methods are only affected by bulk concentration. As a result, ionic conductance of those platforms were unable to change the behavior of charged species on-demand, once the devices were

fabricated. However the IFET can be tunable the surface charge density for ionic conductance.

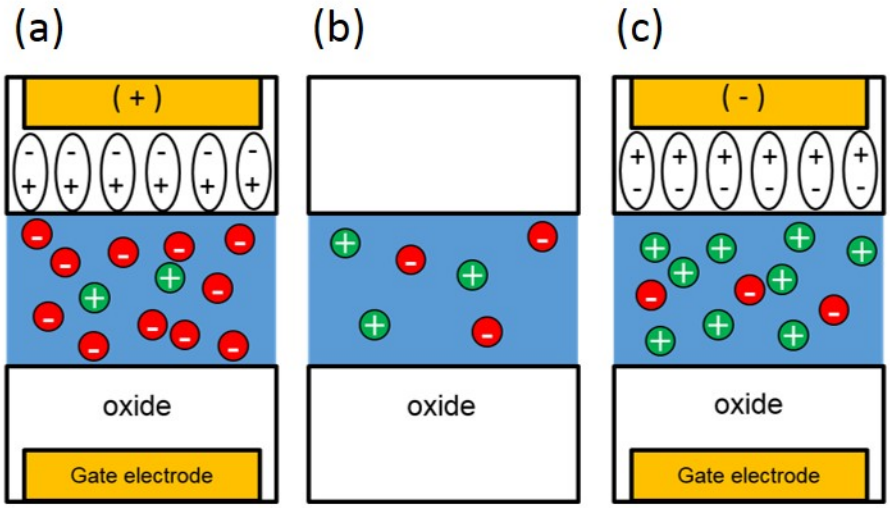

Fig 2.7 Ionic field effect transistor (IFET) mechanism. (a) positive gate potential (b) float gate potential (c) negative gate potential

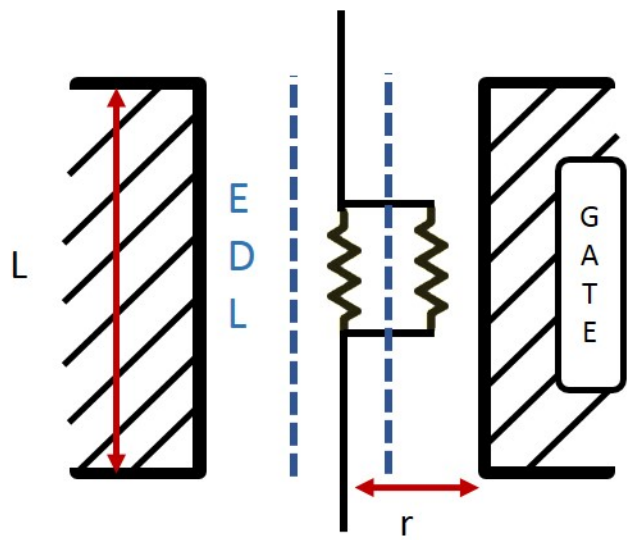

Fig 2.8 The schematic figure of ionic conduction in nanochannel

2.4 conclusion

In this chapter, we mentioned that the IFET device are developed to overcoming the previous methods which change the surface charge of material. However, conventional IFETs have the unipolar behavior unlike the original concept which have the ambipolar behavior. The gate voltage was unable to overcome the polarity of silicon oxide surface charge because silicon oxide have too high surface charge density. We studied the PZC data and dielectric constant to improvement the gate efficiency and tested the leakage current of MOE system to overcome unipolar behavior. As a result, Al_2O_3 is the optimum material instead of SiO_2.

References

(1) Fologea, D.; Uplinger, J.; Thomas, B.; McNabb, D. S.; Li, J. Nano Letters 2005, 5, 1734.

(2) Utkur, M.; Jeffrey, C.; Valentin, D.; Aleksei, A.; Gregory, T. Nanotechnology 2010, 21, 395501.

(3) Wanunu, M.; Meller, A. Nano Letters 2007, 7, 1580.

(4) Stein, D.; Kruithof, M.; Dekker, C. Physical Review Letters 2004, 93, 035901.

(5) Rong, F.; Min, Y.; Rohit, K.; Arun, M.; Peidong, Y. Physical Review Letters 2005, 95, (8), 086607.

(6) Vermesh, U.; Choi, J. W.; Vermesh, O.; Fan, R.; Nagarah, J.; Heath, J. R. Nano Letters 2009, 9, (4), 1315-1319.

(7) Nam, S.-W.; Rooks, M. J.; Kim, K.-B.; Rossnagel, S. M. Nano Letters 2009, 9, (5), 2044-2048.

(8) Karnik, R.; Castelino, K.; Fan, R.; Yang, P.; Majumdar, A. Nano Letters 2005, 5, 1638.

(9) Fan, R.; Huh, S.; Yan, R.; Arnold, J.; Yang, P. Nat Mater 2008, 7, 303-307.

(10) Karnik, R.; Fan, R.; Yue, M.; Li, D.; Yang, P.; Majumdar, A. Nano Letters 2005, 5, 943.

(11) Guan, W.; Fan, R.; Reed, M. A. Nat Commun 2011, 2, 506.

(12) Marek Kosmulski, Lagmuir, 13, 6313 (1997)

(13) https://en.wikipedia.org/wiki/Relative_permittivity

(14) Kim, S. J.; Song, Y.-A.; Han, J. *Chemical Society Reviews* **2010,** 39, 912-922.

Chapter. 3 New design for improving the gate efficiency by all-around-gated IFET

3.1 Introduction

Previous research of IFET have other limitation which is paln gate structure. A planar gate structure in which a gate electrode installed only one wall of nanochannel can modulate the surface charge density at the wall and thus, the efficiency of applying gate potential would become lower than all-around-gate structure which had a gate electrode at entire surface of nanochannels. We calculated unit area capacitances (F/m^2) when the diameter of nanochannel is 10nm and the thickness of oxide wrapped nanochannel is 60nm. We used below two equations (Eq. 3.1, Eq. 3.2).

$$C_{plane} = \frac{\varepsilon_0 \varepsilon_r}{r_b - r_a} \qquad \text{Eq. 3.1}$$

$$C_{cylin} = \frac{\varepsilon_0 \varepsilon_r}{r_a \times ln(\frac{r_b}{r_a})} \qquad \text{Eq. 3.2}$$

Thus, the calculated unit capacitance of cylindrical gate structure have five times larger than plane gate structure.

As previously suggested as "*an ideal structure for field effect reconfigurable nanofluidic diodes would be dual split-gates with a gate-all-around structure and a sub-10 nm nanochannels of a neutral surface*" [1], we have developed a novel design of all-around-gate

structure, with 7.5nm radius nanochannels, with minimal surface charge density using Al_2O_3 which has the surface charge density of $-1.5\ mC/m^2$ in this work.

Firstly, all-around-gate structure was adapted to increase the efficiency of gate effect at least more than 5 times compared to planar-gate structure. This high efficiency led to obtain an ionic field effect at high electrolyte concentration up to 1M. Secondly, we deposited Al_2O_3 which have low surface charge density for enabling a polarity independent control. As a result, our device showed an ambipolar behavior at I_D-V_G measurement. The experimental ambipolar effects were validated by numerical simulation with fringing field effect and counter-ion condensation which had not been considered as major factors. The experimental and numerical results were in line with our logical procedures and well-matched.

3.2 Materials & methods

3.2.1 Fabrication of All-around-Gated Ambipolar IFET

While the fabrication of all-around IFET device was previously reported[2], here we added further process to construct more rigorous all-around IFET device. The fabrication started with bare silicon water (500um thick). On top of the wafer, 1um-thick silicon dioxide (SiO2) and 20nm-thick amorphous Si (a-Si) was sequentially deposited (Figure 3.1 (a)). Using electron beam lithography (EBL) with the e-beam resist of poly methyl methacrylate (PMMA), 80 nanochannels with 50um length were patterned on a-Si (Figure 3.1 (b)). And the reactive ion etching (RIE) was followed to construct a trench structure which will be a nanochannel. That trench had 140nm width and 100nm depth (Figure 3.1 (c)). PMMA was removed by oxygen plasma. Then, SiO_2 was wet anisotropically etched by Buffered Oxide Etchant (BOE) that etches only SiO_2, not a-Si, resulting a circular cross-section of nanochannels (Figure 3.1 (d)). Regardless of the pattern size of a-Si (RIE in Figure 3.1 (e)), the size of nanochannel was determined by BOE in Figure 3.1 (f) which was fixed by the wet etch time of BOE. Because the trench width (RIE) had a large variation due to the limitation of EBL process, this wet etch process satisfied the high reproducibility of nanochannel size.

We named this process as self-limiting process. Transparent Conduct Oxide (TCO) of Aluminum-doped Zinc Oxide (AZO) as gate electrodes was deposited 40nm on the entire surface by Atomic Layer Deposition (ALD) (Figure 3.1 (e)). Transparent AZO was used for the optical observation of substances through nanochannels, while previous work had utilized opaque metal electrodes. To prevent a leakage current through AZO electrode, we partially removed AZO at each end of nanochannel (non-gated region), remaining at the center (10um length called gated region) (Figure 3.1 (f)). The copper electrode pad was patterned on the contact region of AZO gate electrode using e-beam evaporator (Figure 3.1 (g)). Al2O3 dielectric oxide (70nm thickness) was deposited on the entire surface by ALD so that a circular nanochannel with all-around gate electrode could be formed at the center of the trench (Figure 3.1 (h)).

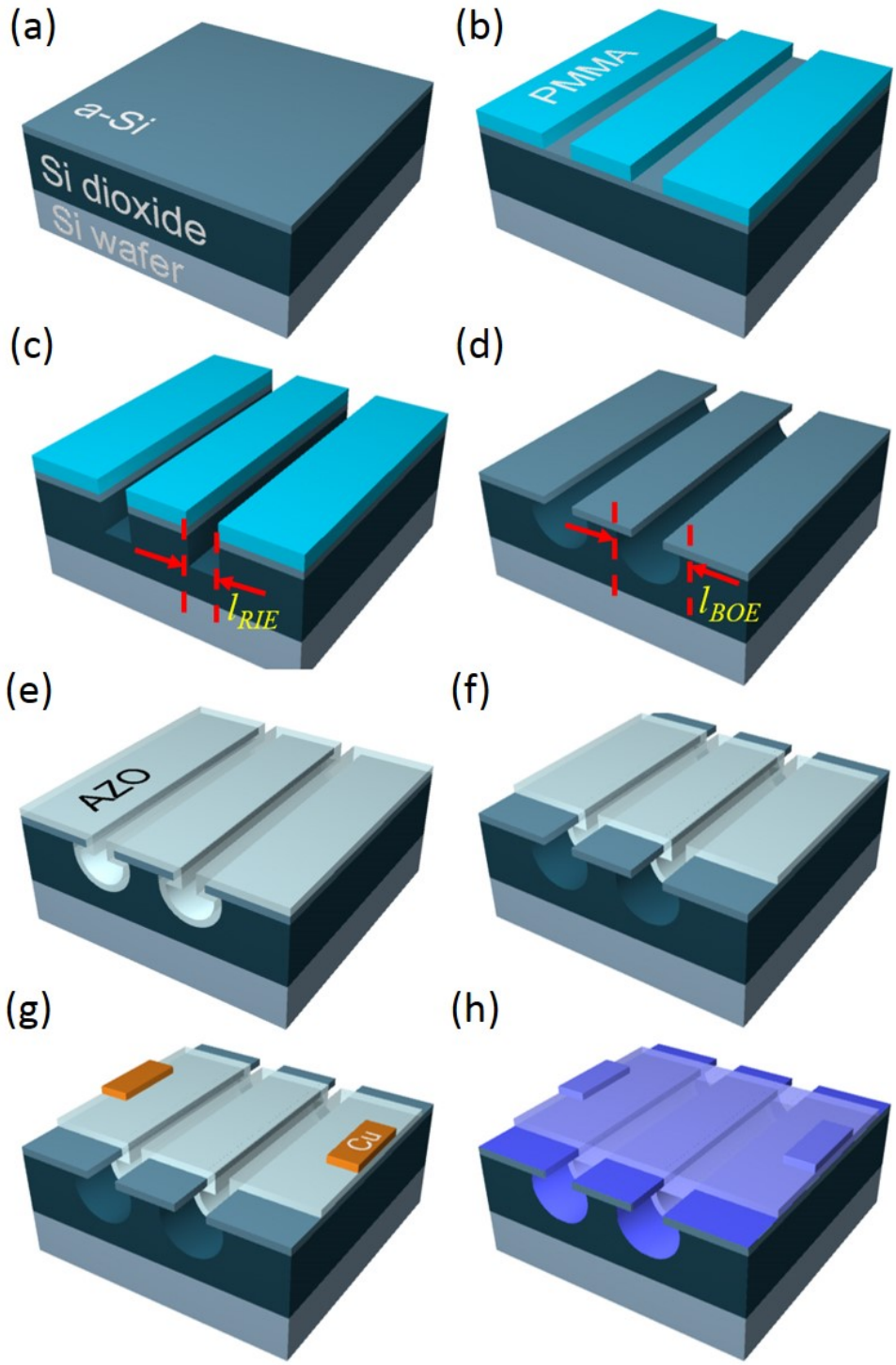

Fig 3.1 Schematics of fabrication process.

3.3 Results and discussion

Figure 3.2(a) showed schematics of fabricated nanochannel. The nanochannel had a constricted area in the middle because a gate electrode existed only at the center of nanochannel. Figure 3.2 (b) and 3.2 (c) showed the SEM image of the cross section of non-gated region (~100nm opening) and gated region (~10nm opening). After deposit SiO_2 (1.5um thickness) on top of Al_2O_3 using plasma enhance chemical vapor deposition (PECVD), microchannels were fabricated near both ends of nanochannel by RIE process so that the microchannels were connected with nanochannels. The microchannels had the dimension of 60um width and 1.5um depth and 5um-radius pillars were installed inside microchannel for preventing a collapse of PDMS cover as shown in Figure 3.2 (d). Finally PDMS cover was bonded using oxygen plasma. The device was heated at 90°C conformal bonding. Figure 3.2 (d) showed the assembly device with magnified microscopic view near the nanochannel. Note that the color of AZO electrode (a pink color) could be observed through nanochannel array so that we confirmed the nanochannels in this work had an optical transparency.

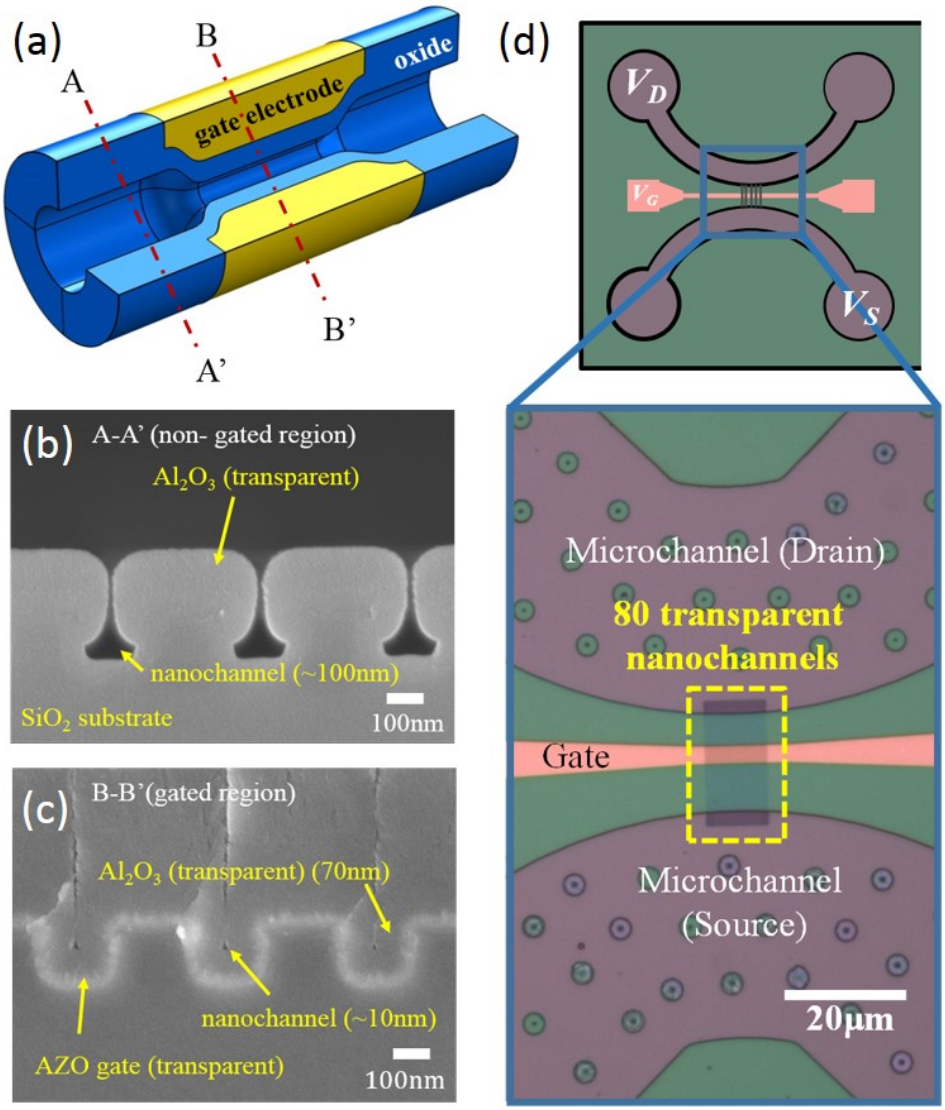

Fig 3.2 (a) The schematic diagram of all-around-gated IFET. Cross-sectional SEM images of (b) non-gated region and (c) gated region. (d) Microscopic image of IFET device near nanochannel array.

3.4 Conclusion

In this chapter, we developed the design of all-around-gate structure to improve the gate efficiency of conventional plane gate structure. We calculated the gate efficiency between plan gate structure and all-around-gate structure using unit area capacitance equation. As a result, the calculated unit capacitance of cylindrical gate structure have five times larger than plane gate structure.

We fabricated the nanochannel device insulted all-around-gate structure using electron beam lithography and atomic layer deposition. The device have 7.5nm diameter and 100um nanochannel length and 80 arrays.

References

(1) Guan, W.; Fan, R.; Reed, M. A. Nat Commun 2011, 2, 506.

(2) Nam, S.-W.; Rooks, M. J.; Kim, K.-B.; Rossnagel, S. M. Nano Letters 2009, 9, (5), 2044-2048.

Chapter 4. Theory of IFET

4.1 Governing equations of nanofluidics

Poisson-Nernst-Planck-Stokes formulation is valid in the system because the validity of the continuum frameworks is held down to a length scale greater than 1nm[1]. Independent variables are electrostatic potential (ψ), ion concentration of i-th species (c_i), pressure (p), and flow field ($\mathbf{u}$) obtained by following equations,

$$-\varepsilon_f \nabla^2 \psi = \rho_e = F\sum_i Z_i c_i, \qquad \text{Eq. 4.1}$$

$$0 = -\nabla \cdot \mathbf{J}_i, \qquad \text{Eq. 4.2}$$

$$\mathbf{J}_i = -D_i \nabla c_i - \frac{Z_i F D_i}{RT} c_i \nabla \psi + c_i \mathbf{u}, \qquad \text{Eq. 4.3}$$

$$0 = -\nabla p + \eta \nabla^2 \mathbf{u} - \rho_e \nabla \psi, \qquad \text{Eq. 4.4}$$

$$\text{and } \nabla \cdot \mathbf{u} = 0 \qquad \text{Eq. 4.5}$$

where ε_f is the electrical permittivity of the electrolyte, ρ_e is the volumetric charge density, F is Faraday constant, Z_i is valence of i-th species, D_i is diffusivity of i-th species, R is gas constant, T is temperature, and η is the dynamic viscosity. Poisson equation represented by equation Eq. 4.1 describes the electrostatic potential distribution. Nernst-Planck equations represented by equation Eq. 4.2 in which ionic molar flux $\mathbf{J}_i$ is expressed in equation Eq. 4.3

describes the mass transport of charged species under consideration of the diffusion, the electromigration and the convection. Stokes equations and continuity equation represented by equation Eq. 4.4 and Eq. 4.5 describe the fluid flow. Equations 4.1 ~ 4.5 should be solved by coupling manner.

4.2 General description for metal-oxide-electrolyte (MOE) system

In usual MOE system, the surface charge density is obtained from simple algebraic equations independent from governing equations. In various literatures[2-5], the MOE system was approximated to series capacitors by equivalent electrokinetic circuit models. Using those models, zeta potential and surface charge density modulated by gate voltage can be analyzed by solving simple algebraic equations. However, those equations are only valid in the planar-type MOE system. Therefore, those models should be reformulated to be applicable to the cylindrical MOE system which is our system. When the Stern layer on the charging behavior of the MOE system can be described by the following set of 1D ordinary differential equations based on Gouy-Chapmann theory in case of symmetric electrolyte.

$$\frac{1}{r}\frac{\mathrm{d}}{\mathrm{d}r}\left(r\frac{\mathrm{d}\varphi}{\mathrm{d}r}\right)=\frac{2ZFc_0}{\varepsilon_f}\sinh\left(\frac{ZF\varphi}{RT}\right) \quad \text{at } 0<r<R_f \qquad \text{Eq. 4.6}$$

$$\frac{1}{r}\frac{\mathrm{d}}{\mathrm{d}r}\left(r\frac{\mathrm{d}\Phi}{\mathrm{d}r}\right)=0 \quad \text{at } R_f<r<R_f+d_{ox} \qquad \text{Eq. 4.7}$$

In the above, φ is the electric potential in electrolyte, Φ is the electric potential in oxide layer, R_f is the radius of the nanofluidic channel, d_{ox} is the oxide layer thickness, and Z is ion valence. Equation 4.6 is the Poisson-Boltzmann equation expressed as cylindrical form to describe the potential distribution inside nanochannel and equation 4.7 is the Laplace equation describing the potential distribution within oxide layer. Because we neglect the Stern layer, zeta potential is approximately equal to surface potential, $\zeta=\varphi|_{Rf}$, directly given by gate voltage, V_G. Thus, the modulated zeta potential corresponding to V_G can be obtained by solving equations 4.6 and 4.7 with following boundary conditions. (Figure 4.1 shown the schematic figure of IFET)

$$\frac{\mathrm{d}\varphi}{\mathrm{d}r}=0 \qquad \text{at } r=0 \qquad \text{Eq. 4.8}$$

$$\varphi=\Phi \qquad \text{at } r=R_f \qquad \text{Eq. 4.9}$$

$$-\varepsilon_f\frac{\mathrm{d}\varphi}{\mathrm{d}r}+\varepsilon_{ox}\frac{\mathrm{d}\Phi}{\mathrm{d}r}=\sigma_0 \qquad \text{at } r=R_f \qquad \text{Eq. 4.10}$$

$$\Phi = V_G \qquad \text{at } r = R_f + d_{ox} \qquad \text{Eq. 4.11}$$

where ε_{ox} is the electrical permittivity of the oxide layer and σ_0 is the inherent surface charge density on oxide/electrolyte interface which is near-zero value in our ambipolar IFET system, while the typical value of σ_0 is high enough to have unipolar electrical response[6, 7]. Equation 4.8 is the condition for axis of symmetry, equations 4.9 and 4.10 describe oxide/electrolyte interface, and equation 4.8 is the voltage condition by gate electrode. Equation 4.10 implies the discontinuity of electric displacement field at interface where Gauss's law for electrostatic field should be satisfied. Since above formulation is valid to a system where the full length of nanochannel is completely covered by a gate electrode with low gate voltage (fully-gated IFET), we need additional considerations for the partial coverage of gate electrode (partially-gated IFET) as shown in Figure 3.2 (a) with high gate voltage. The considerations are a fringing field effect and a counter-ion condensation as following.

Fig 4.1 The schematic figure of electrical potential distributiona of IFET device cross section and expression equations.

4.3 Fringing field effect

Despite of difference in structure, the zeta potential modulation of partially-gated IFET (Fig 4.2 (b)) could be similar to that of fully-gated IFET (Fig 4.2 (a)) in physical intuition. Define 'gated region' as a region of gate electrode and 'non-gated region' as a region of absence of that. Gated and non-gated regions correspond to 'A-A'' and 'B-B'' denoted in Figure 3.2 (a), respectively. Typically, when voltage is applied to the gate electrode, the electric field is sought to be generated only inside the oxide layer of gated region and the electric field abruptly drops to zero in that of non-gated region. However, this is impossible because of the conservative nature of the electric field, $\nabla \times \mathbf{E} = \mathbf{0}$[8]. To satisfy the conservation, the electric field should curve and extend outward into non-gated region which is called fringing field effect or edge effect. Due to this fringing field, the zeta potential on oxide/electrolyte interface of non-gated region can be modulated as similar as gated region. The impact of fringing field was researched by Lin et al[9] using carbon nanotube FET (CNFET) where fringing field affected gating phenomena significantly. To solve fringing field directly, it requires high-cost computation. Numerical domain must be discretized into nearly zero sized elements in the vicinity of the each gate end, so that the number of degree of freedom diverges (Fig 4.2 (c)). To avoid this, we assumed that the distribution of the modulated zeta potential along the nanochannel wall followed the Gaussian

distribution expressed as

$$f(x)=\frac{A}{\sigma\sqrt{2\pi}}\exp\left[-\frac{(x-\mu)^2}{2\sigma^2}\right] \qquad \text{Eq. 4.12}$$

where A is an arbitrary constant, σ is the standard deviation, and μ is the mean value of the arbitrary function $f(x)$, respectively. Using equation 4.12, the modulated zeta potential along the channel walls was set to be

$$\zeta(z)=\begin{cases}\zeta_{gate}\exp\left[-\dfrac{\left(z+\frac{L_{gate}}{2}\right)^2}{\alpha^2}\right] & \text{at} \quad z<-\dfrac{L_{gate}}{2} \text{ (region B)} \\ \zeta_{gate} & \text{at} \quad -\dfrac{L_{gate}}{2}\le z\le\dfrac{L_{gate}}{2} \text{ (region A)} \\ \zeta_{gate}\exp\left[-\dfrac{\left(z-\frac{L_{gate}}{2}\right)^2}{\alpha^2}\right] & \text{at} \quad z>\dfrac{L_{gate}}{2} \text{ (region B)}\end{cases}.$$

Eq. 4.13

In above expressions, ζ_{gate} is the modulated zeta potential on oxide/electrolyte interface by gate electrode which is calculated from equations 4.6 ~ 4.11. α^2 is defined as $\alpha^2 = (L_{channel}-L_{gate})^2/4\ln\beta$ in which $L_{channel}$ is the length of the nanochannel, L_{gate} is the length of the gated region and $\beta = \zeta_{gate}/\zeta_{min}$ is ratio of modulated zeta

potential and its minimum zeta potential at the end of nanochannel wall. Since β is a phenomenological parameter, one can choose it in the range of 1 to ∞. For example of the limiting cases, β is equal to 1, corresponding to fully gated system and β goes to infinity, diminishing the fringing field effect. We postulated that β was proportional to the electrical conductivity of the electrolyte solution and its values were summarized in Table 4.1

Table 4.1 Used parameters to describe a fringing field effect and a counter-ion condensation

c_0 [M]	β	ν
10^{-5}	20	0.005
10^{-4}	200	0.05
10^{-3}	2,000	0.5
10^{-2}	20,000	2
10^{-1}	200,000	2
1	2,000,000	2

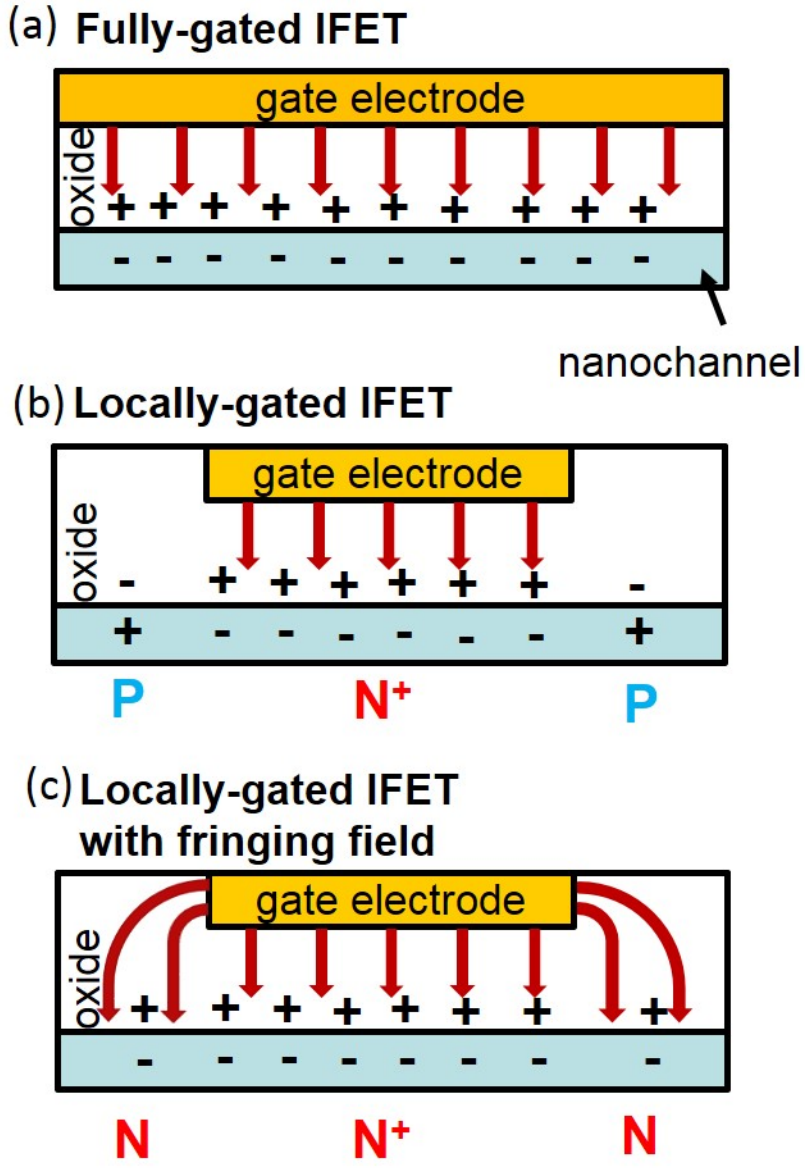

Fig 4.2 the zetapotential distribution of (a) fully-gated IFET, (b) Locally-gated IFET, (c) Loaclly-gated IFET with firinging field.

4.4 Counter-ion condensation

Surface charge density, σ_s can be determined from the modulated zeta potential if charge-potential relation in electrokinetic system is known. In classical viewpoint, the Grahame equation based on the Poisson-Boltzmann equation can be used to determine the surface charge density (Fig 4.3 (a)). However, when zeta potential exceeds the thermal voltage, $RT/F \approx 25$mV, the electric double layer starts to enter a non-linear regime where the Grahame equation is expected to break down[2, 10, 11] (Fig 4.3 (b)). Under these conditions such as high zeta potential or high electrolyte concentration, one should consider the ion-ion interactions so that surface charge over-screening and ion crowding are arose in the vicinity of the solid/electrolyte interfaces. To elucidate those non-linear effects, additional compact layer consist of counter-ions has been proposed[10, 12]. In those literatures, counter-ions in the vicinity of the highly charged surface are condensed in narrow layer, and then new compact layer is formed beyond the Stern layer. Consequently, the impact of highly charged surface to the electric double layer structure is reduced by condensed counter-ions. To obtain charge-potential relation in that non-linear regime, Kilic and coworkers established the analytical model based on the modified Poisson-Boltzmann equation with a phenomenological parameter[10] which we chose in this work.

In their model, parameter ν represents the ratio of bulk

electrolyte concentration (c_0) and maximum condensed concentration (c_{max}) expressed by

$$\nu = \frac{2c_0}{c_{max}} = 2a^3 N_A c_0 \qquad \text{Eq. 4.14}$$

Where N_A is the Avogadro number and a is the effective diameter of an ion. Note that a is not necessarily the actual diameter (~O (1) Å), it just means ion-ion correlation under phenomenological viewpoint. By definitions of Eq. 4.14, ν has a maximum value, 2 because c_0 cannot exceed the maximum concentration, c_{max}. By theoretical derivation without loss of generality, charge-potential relation became following form,

$$\sigma_s = 2\,\mathrm{sgn}(\zeta) ZFc_0\lambda_D \sqrt{\frac{2}{\nu}\ln\left[1 + 2\nu \sinh^2\left(\frac{ZF\zeta}{2RT}\right)\right]} \qquad \text{Eq. 4.15}$$

where λ_D is the Debye layer thickness defined as $\lambda_D = \sqrt{(\varepsilon_f RT)/(2Z^2F^2c_0)}$, sgn($\zeta$) is sign of the zeta potential, and ζ is calculated from equation 4.15. Due to highly confined nanostructure (radius in O(10)nm), ion-ion correlation were expected to be strong. To capture the strong correlation, the effective diameter of an ion, a, was fixed to be 7.5nm[10], so that ν was proportional to the bulk electrolyte concentration from equation 4.15 of which values were summarized in Table 4.1

4.5 Ionic current

To obtain theoretical *I-V* characteristics of IFET, local ionic current density, **i,** is defined by

$$\mathbf{i} = \sum_j Z_j F\left(- D_j \nabla c_j - \frac{Z_j F D_j}{RT} c_j \nabla \psi + c_j \mathbf{u} \right) \qquad \text{Eq. 4.16}$$

and then total ionic current through IFET system (I) can be calculated by

$$I = N_{ch} \int_S \mathbf{i} \cdot \mathbf{n} \mathrm{d}S \qquad \text{Eq. 4.17}$$

where N_{ch} is the number of nanochannel, S is arbitrary cross section of the system, and **n** is normal vector on surface S. Required field quantities in equation 4.16 were obtained from equation 4.1 ~ 4.15.

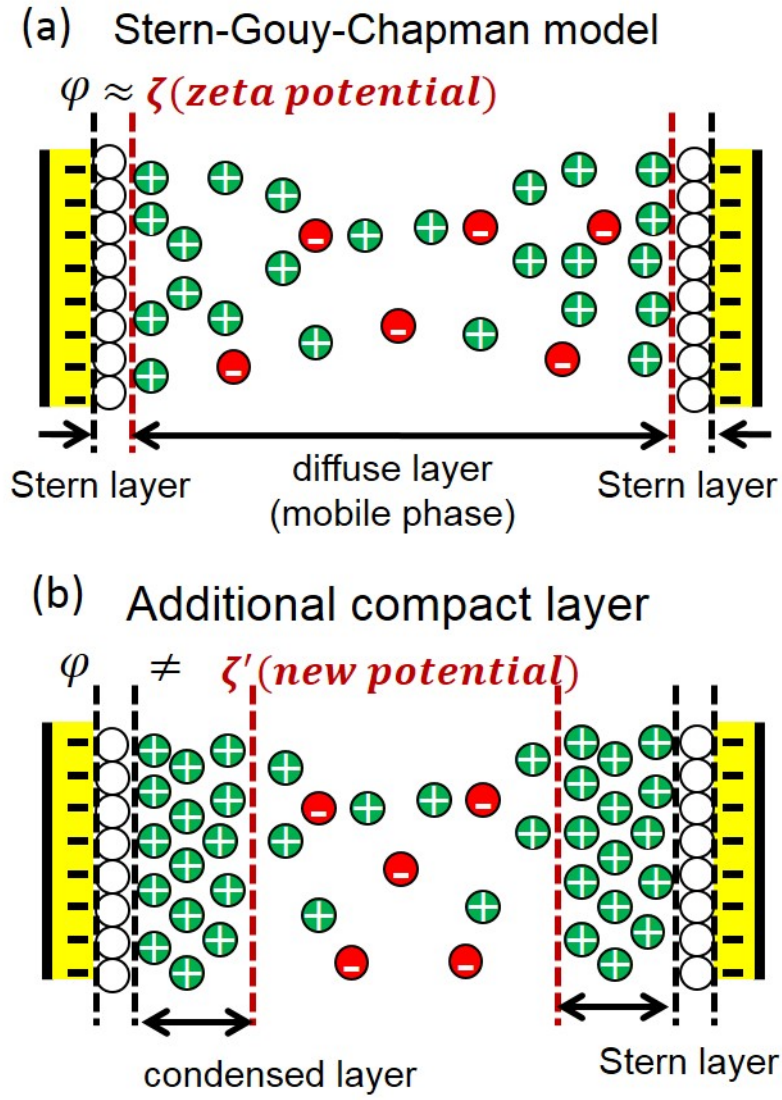

Fig 4.3 the zetapotential distribution of (a) fully-gated IFET, (b) Locally-gated IFET, (c) Loaclly-gated IFET with firinging field.

Reference

(1) Bocquet, L.; Charlaix, E. Chemical Society Reviews 2010, 39, (3), 1073-1095.

(2) Jiang, Z.; Stein, D. Langmuir 2010, 26, (11), 8161-8173.

(3) Jiang, Z.; Stein, D. Physical Review E 2011, 83, (3), 031203.

(4) Yeh, L.-H.; Xue, S.; Joo, S. W.; Qian, S.; Hsu, J.-P. The Journal of Physical Chemistry C 2012, 116, (6), 4209-4216.

(5) Hughes, C.; Yeh, L.-H.; Qian, S. The Journal of Physical Chemistry C 2013, 117, (18), 9322-9331.

(6) Karnik, R.; Fan, R.; Yue, M.; Li, D.; Yang, P.; Majumdar, A. Nano Letters 2005, 5, 943.

(7) Rong, F.; Min, Y.; Rohit, K.; Arun, M.; Peidong, Y. Physical Review Letters 2005, 95, (8), 086607.

(8) Wangsness, R. K., Electromagnetic fields. Wiley: 1986.

(9) Lin, Y.-M.; Appenzeller, J.; Avouris, P. Nano Letters 2004, 4, 947.

(10) Kilic, M. S.; Bazant, M. Z.; Ajdari, A. Physical Review E 2007, 75, 021502.

(11) Russel, W. B.; Saville, D. A.; Schowalter, W. R., Colloidal Dispersions. Cambridge University Press: 1992.

(12) Manning, G. S. The Journal of Physical Chemistry B 2007, 111, 8554.

Chapter. 5 Analysis of all-around-gated ambipolar IFET

5.1 Introduction

Recent advances in nano-fabrication methods enable to fabricate rigorous and definite nano-sized structure for various scientific and engineering applications. Nanostructure possesses unique scientific and technological properties that microstructure cannot exhibit. Especially, as decreasing the size of nanostructure below 100nm, the structure had a perm-selectivity which let only counter-ions can pass through below a critical electrolyte concentration. The perm-selectivity was reported to be depending on the magnitude and polarity of surface charge density and bulk electrolyte concentration. Thus, the active control of the surface charge density at wide range of electrolyte concentration has been drawn significant attentions in both scientific and engineering field[1-6] for manipulating the motion of charged species and this has become the essence of nanofluidics research. The emerging application fields of nanofluidc system were energy harvesting[1, 2], biosensors[3, 4], backflow from shale gas extraction port[5] or desalinations of seawater[6] which enable to create a huge market that never have existed. Those applications were fundamentally originated from controlling the motion of charge species passing through a nanostructure and, therefore, the cost-effective/on-demand/sensitive control has become the most important practical issue of nanofluidic researches.

5.2 Materials and methods

5.2.1 Electrical measurement method of IFET

We measured the ionic current (I_D) for different gate voltage (V_G) with KCl buffer solution at pH 7 in the concentration range from 10^{-5}M to 1M. The fluidic chambers were covered with PDMS and Ag/AgCl electrodes were connected on both sides of the chambers. We measured the electric data using the parameter analyzer (Agilent 4156C) in the homemade dark box which blocked the electrical noise. (Figure 5.1 (b)) The current was measured as follows. First, drain voltage (V_D) increased from 0V to +2V at 0.25V/min for low concentration and 0.5V/min for high concentration, respectively. After 5min delay time, V_D decreased from 0V to -2V at the same voltage step. For each concentration of KCl, the microchannel was refreshed for 10 minutes with the same solution using a rotary pump. The measurements without the application of gate voltage were repeated until the results were reproduced. For a high concentration case such as 10^{-1}M and 1M, serious precipitation occurred inside the microchannels. To prevent it, we added refresh step at each change of gate voltage. Leakage current (a current from source to gate) was simultaneously measured for confirming the proper operation. (Figure 5.1 (a))

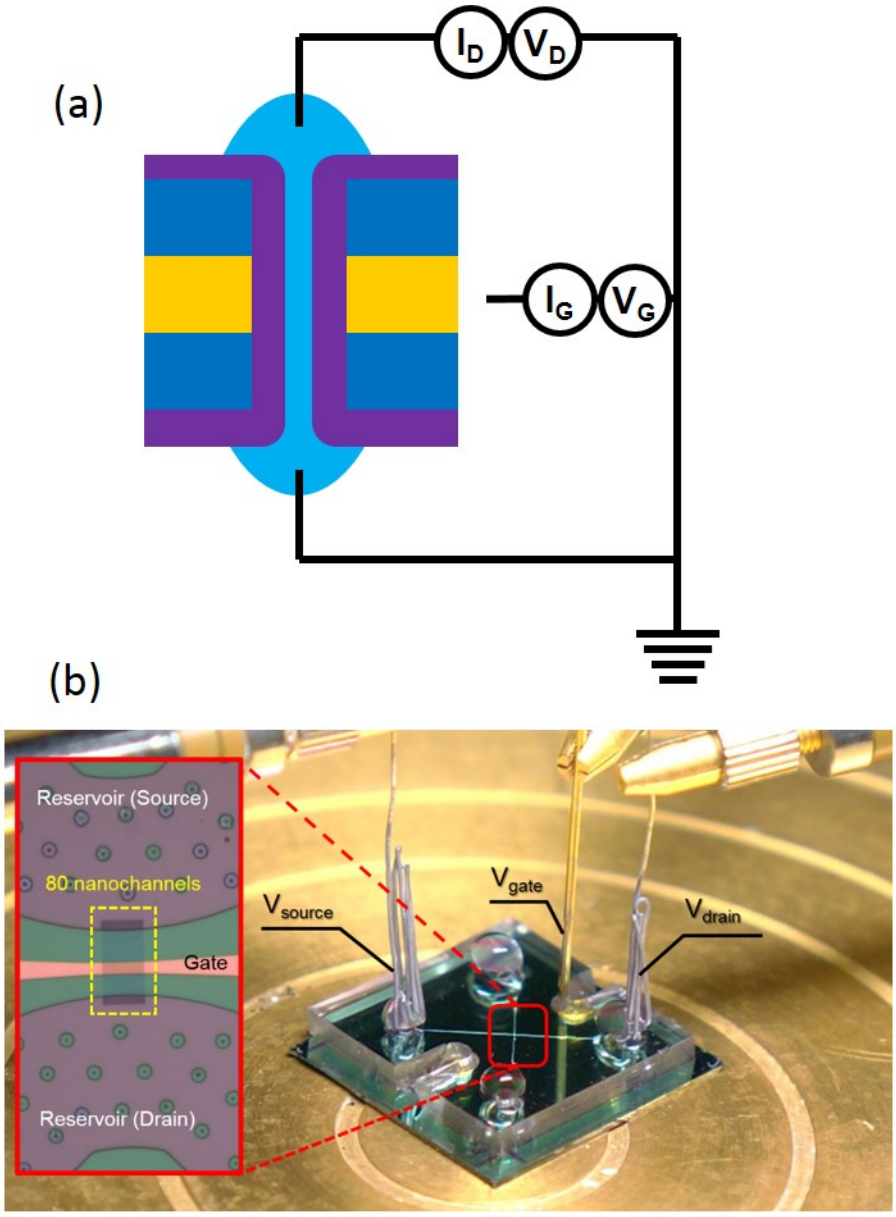

Fig 5.1 (a) The schematic figure of electric circuit of IFET measurement (b) photograph of measurement setup

5.3 Results and discussion

5.3.1 Ionic conductance at floating gate

Ionic transport in nanofluidic system has the unique property of surface-charge-governed regime demonstrated by D. Stein *et al.*[7] In a dilute limit, ionic conductance is independent from the bulk properties of the system such as the electrolyte concentration or the geometrical factor, so that the conductance curve saturates below a specific concentration value which is determined by surface charge density and called 'surface-charge-governed conductance'. Because the plateau of conductance curve is only revealed in nanochannel system, this property has been utilized to demonstrate the validity of the device in the view point of nanofluidic application. Beyond the specific concentration value, the conductance is proportional to the bulk concentration, called geometry-governed regime. These two distinct regimes can be plotted (ionic conductance as a function of bulk concentrations) simultaneously as shown in Figure 5.2. In a cylindrical nanochannel, the analytical expression of ionic conductance, G, was derived[8] as

$$G = \frac{\pi}{4}\frac{d_{nano}^2}{L_{nano}}\left[\left(\mu_{co} + \mu_{counter}\right)c_0 F + \mu_{counter}\frac{4|\sigma_0|}{d_{pore}}\right] \qquad \text{Eq. 5. 1}$$

Where d_{nano} is the diameter of a nanochannel, L_{nano} is the length of a nanochannel, and μ_{co} and $\mu_{counter}$ is the electrophoretic mobility of co- and counter-ion, respectively. The first term in equation Eq. 5.1 represents the bulk conductance and the second term represents the surface-charge-governed conductance. Using equation 5.1 and circuit theory, the total conductance of our IFET at floating gate, G_{total}, was calculated from $G_{total}=80\times(G_{gated}\times G_{non-gated})/(2G_{gated}+G_{non-gated})$ in which G_{gated} and $G_{non-gated}$ are the ionic conductance of gated and non-gated region, respectively. We used values of μ_{co} $=7.853\times10^{-8}m^2/V\cdot s$, $\mu_{counter}$ $=7.582\times10^{-8}m^2/V\cdot s$, $|\sigma_0|=1.5mC/m^2$, $d_{nano}=15nm$ (gated region) and 100nm (non-gated region), and $L_{nano}=10$ um (gated region) and 5um (non-gated region). Both theoretical (solid line) and experimental (circles) conductance as a function of bulk concentration were shown in Figure 5.2. In a low concentration range ($c_0<10^{-4}M$), experiments were saturated to the surface-charge-governed conductance and consistent with analytical solution and the conductance fell into the geometry-governed regime above the concentration. However, in a high concentration range, *i.e.* $c_0>10^{-1}M$, the experiments were shown to be deviated from the theoretical calculation, while previous literatures followed the theoretical calculation over 1M concentration[7, 8, 9]. The discrepancy would be come from highly confined microchannel. Our microchannels had the thickness of

1.5 um, while previous studies usually provided the demonstration with an open reservoir. The thin microchannel could provoke strong ion-ion interaction or ion-wall interaction in a high concentration range so that KCl solution at 100mM and 1M concentration turned into a solid precipitation that hindered the ionic current through the micro-nanochannel.

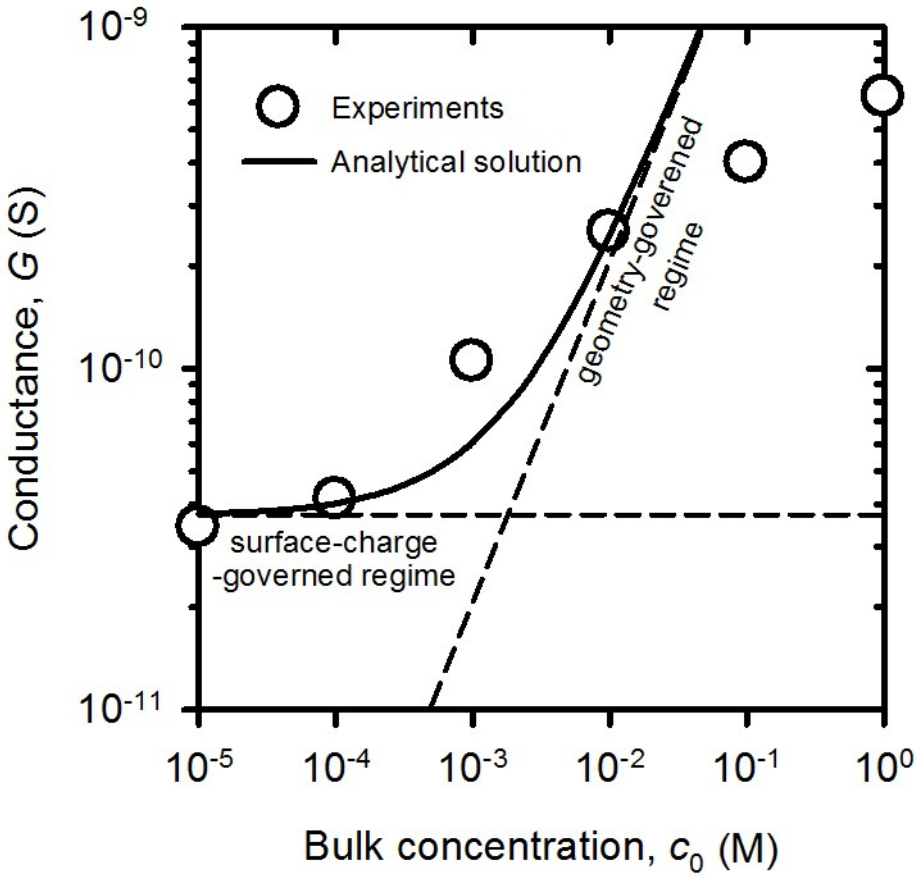

Fig 5.2 Ionic conductance as function of bulk concentration. Experimental conductance and analytical solutions were denoted by open circles and solid line, respectively. The plot clearly demonstrated a nanofluidic characteristic of surface-charge- and geometry-governed regime

5.3.2 The formation of precipitation with high KCl concentration

In spite of the discrepancy in high concentration range, we concluded that our device was intact because surface-charge-governed conductance as the unique property of nanofluidic system was observed.

After the electrical measurement with the KCl solution of concentration over 10^{-1}M, serious precipitations were accumulated at the microchannel as shown in Figure 5.3 The precipitation decreased the cross-sectional area of microchannel so that an ionic current significantly decreased.

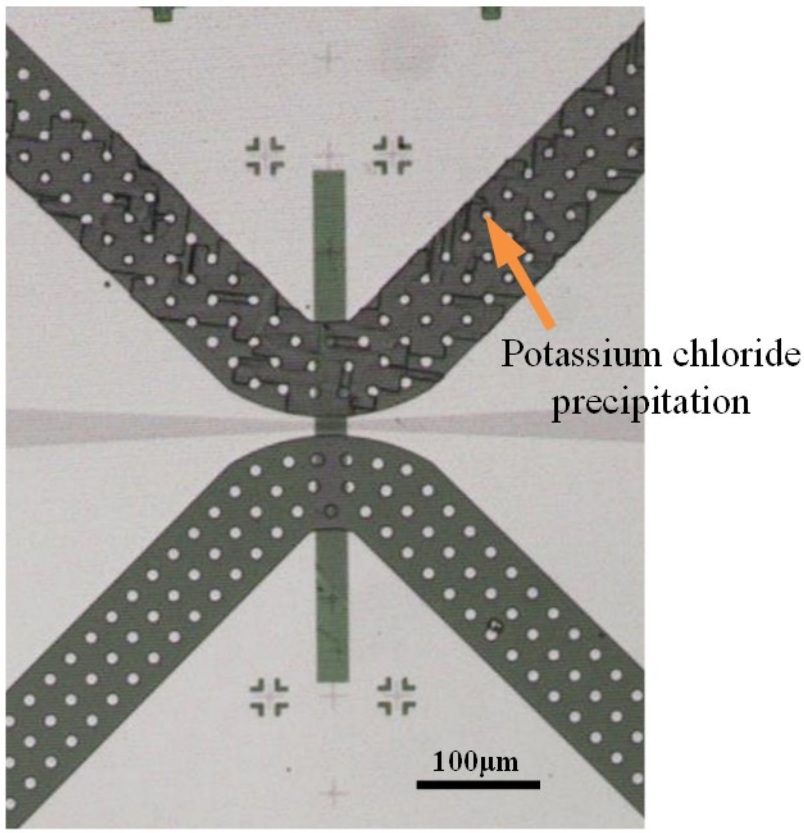

Fig 5.3 The formation of KCl precipitation after the experiment with 10^{-1}M and 1M KCl solution.

5.3.3 Ionic current with gate voltage

The ionic currents (I_D vs V_D) were measured as a function of gate voltage (V_G) at the concentration range from 10^{-5}M to 1M as shown in Figure 5.4, demonstrating the Ohmic (or linear) relationship between I_D and V_D within the voltage range of $|V_D|<2$V. Over the range, one can have ion concentration polarization phenomena which involve a non-linear current-voltage relationship[10, 11]. Higher KCl concentration, we obtained higher ionic current values. Upon the application of gate voltage, ionic conductance increased regardless the polarity of gate voltage for entire concentration range, called ambipolar behavior. A terminology of 'ambipolar' in MOSFET (Metal-Oxide-Semiconductor Field-Effect Transistor) represents that the channel polarity strong depends of the polarity of gate voltage. For instance, negative gate voltage induces abundant holes inside the channel, so that the channel becomes positive polarity and vice versa. In case of IFET, the same mechanism would be hold with near-zero surface charge. Thus, the increment of ionic current was proportional to the absolute value of the gate voltage. On the contrary, the ionic current should increase with either positive or negative gate voltage, if the IFET had unipolar characteristics. The ambipolar behavior was originated from that the nanochannel had extremely low surface charge density due to Al_2O_3 layer and the gate electrode had so-called an "all-around-gate structure" for the high sensitivity.

5.3.4 Leakage current of IFET device.

In order to show the robustness of the system, we simultaneously measured the leakage current from source to gate. Figure 5.5 showed that the leakage currents were below 4pA and independent from the bulk concentrations, leading to a conclusion that the leakage current would not effect on the ionic currents through source to drain. Additionally, the same order of leakage current in whole concentration range taught us that our device successfully worked without dielectric breakdown.

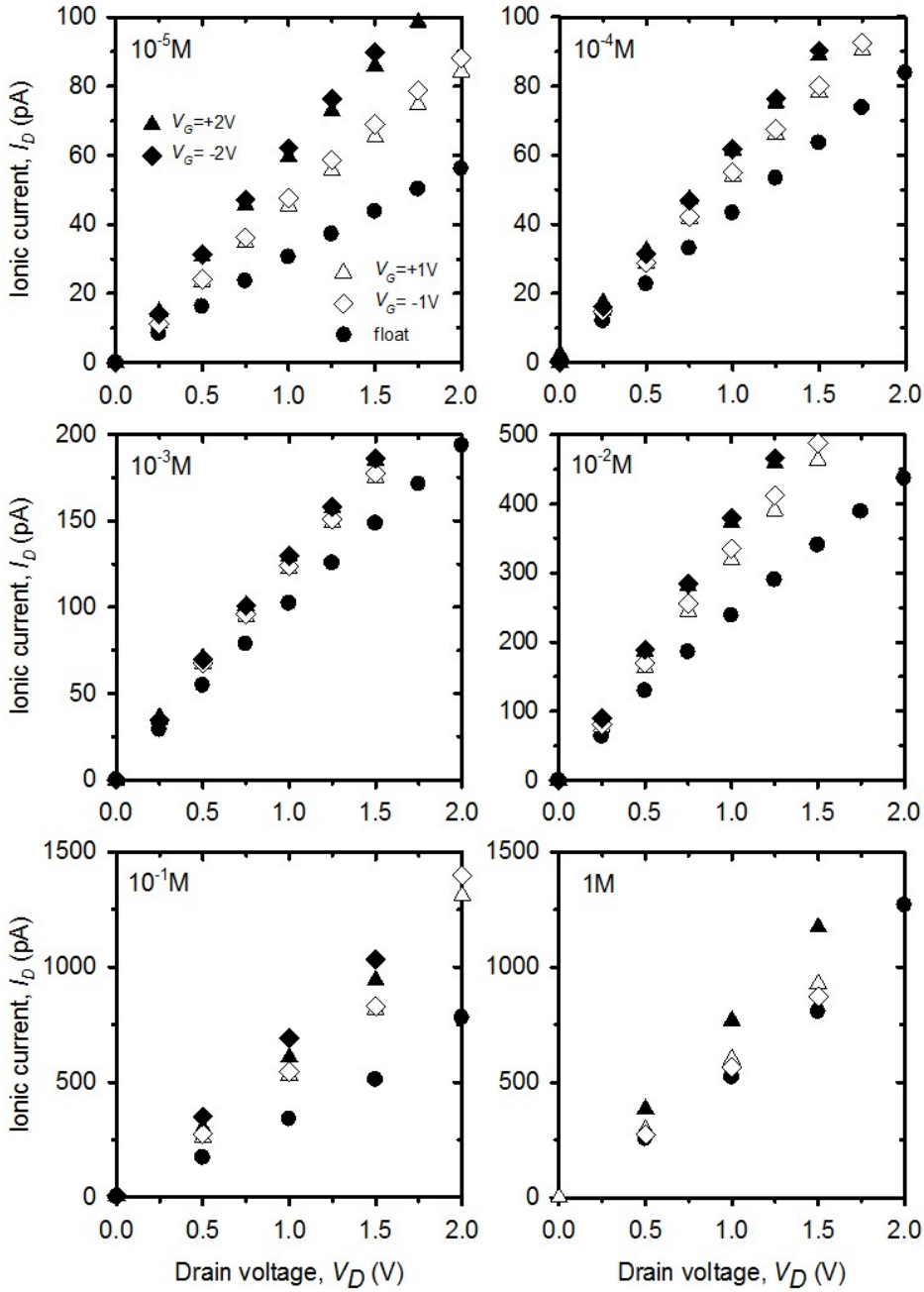

Fig 5.4 Experimentally measured I_D– V_D characteristics in the concentration range of 10^{-5}M to 1M. The conductance increased as a function of the absolute value (regardless of the polarity) of V_G.

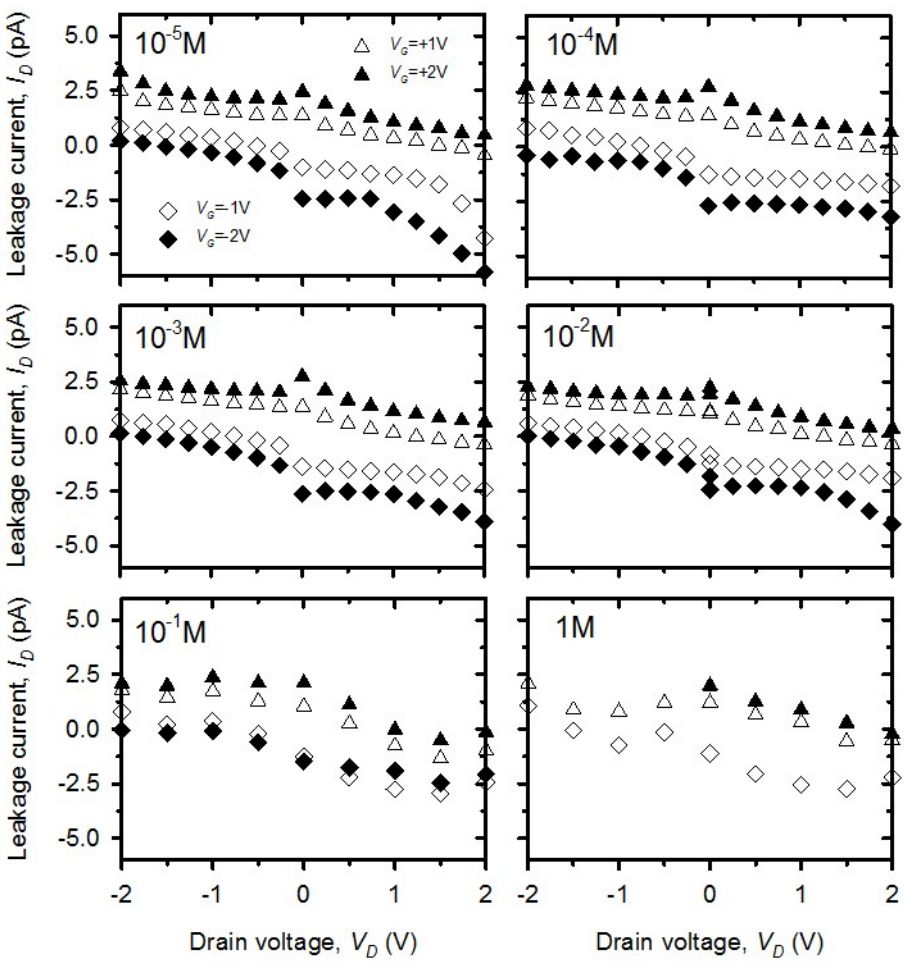

Fig 5.5 Leakage current as a function of drain voltage in the concentration range of 10^{-5}M to 1M.

5.3.5 Ambipolar characteristics (I_D- V_G as a function of V_D): Numerical matching

In an ambipolar IFET device, I_D- V_G characteristics become V-shaped curves since the ionic current should be modulated regardless of the polarity of gate voltage. On the contrary, a unipolar IFET has a diode behavior. The measured I_D- V_G characteristics were plotted in Figure 5.6 for different electrolyte concentrations with numerical results. The measured I_D- V_G characteristics were ambipolar (V-shaped curve) since an inherently low surface charge density of Al_2O_3 (-1.5mC/m^2) and higher capacitance of an all-around-gate structure (~5 times) than that of a planar-gate effectively reflected the gate polarity.

In a low (10^{-5}M ~ 10^{-4}M) and an intermediate (10^{-3}M ~ 10^{-2}M) concentration range, numerical results were well-matched with experimental data. For 10^{-5}M and 10^{-4}M, the extent of the ionic current modulation was appeared in the same order of magnitude because those concentrations were in surface-charge-governed regime[7] where ion transport through the nanochannel is affected only by the surface charge density of nanochannel rather than bulk property. Meanwhile, deviations between measured and numerical results occurred in high concentration range (10^{-1}M ~ 1M). Higher the bulk concentration gave larger deviation. Nevertheless, the measured I_D- V_G characteristics plotted in Figure 5.6 were ambipolar.

Consequently, more constraints in theoretical considerations would be needed to describe the ion transport at extremely high concentration

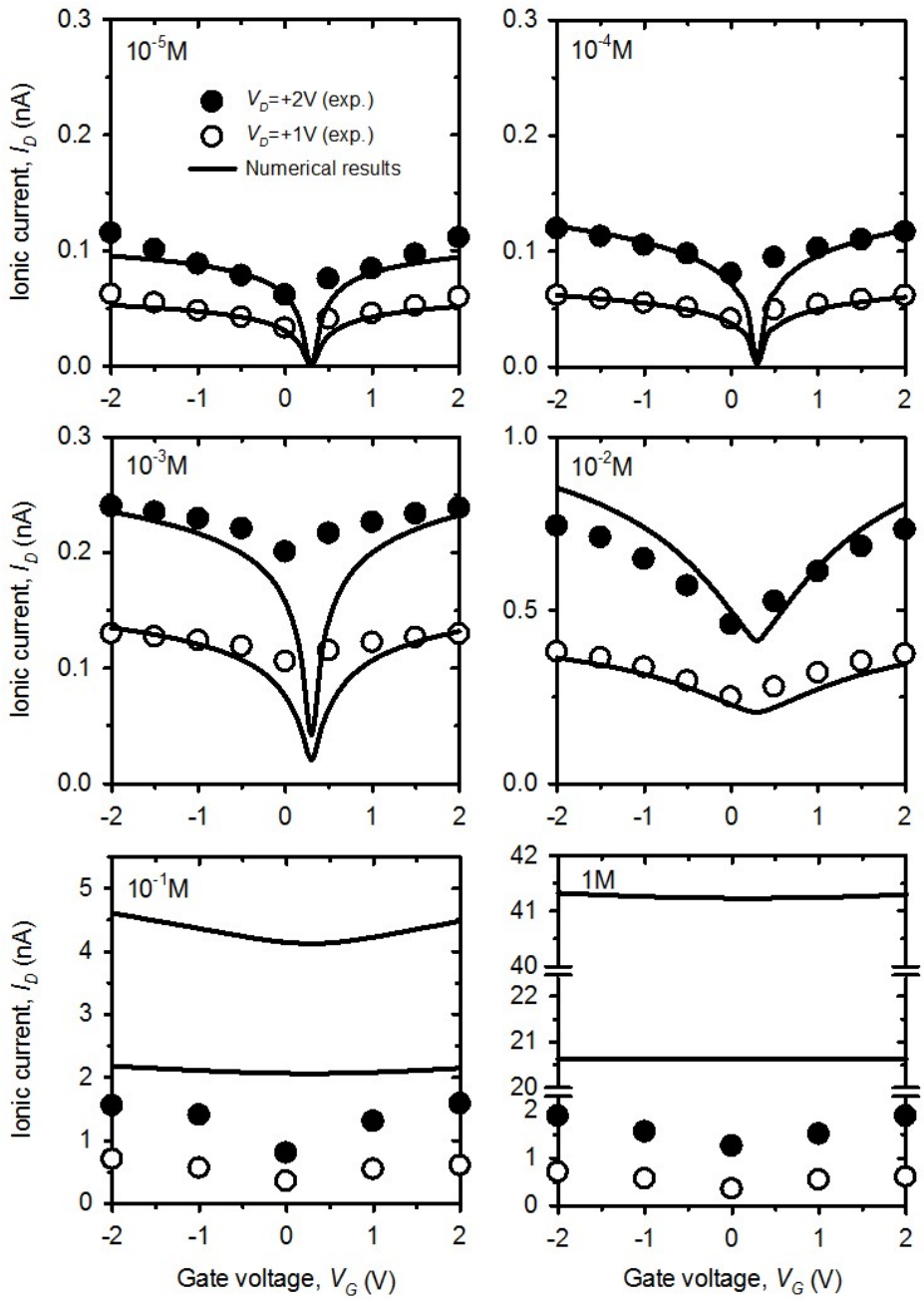

Fig 5.6 Experimental and numerical I_D– V_G at each electrolyte concentration. The "V" shape represented the ambipolar behavior.

5.3.6 The effects of fringing field and counter-ion condensation

We had adopted two additional constraints which were fringing field effect and counter-ion condensation to describe the ionic transportation through the partially gated IFET. Compared to Poisson-Nernst-Planck-Stokes formulation without any constraints (dashed line in Figure 5.7), our modified formulation (solid line) was well-matched with experimental results. With a view point of PNPS formulation without constraints, a positive gate voltage changed the polarity of gated region only, and then nanochannel behaved as the npn nanofluidic transistor for negatively charged nanochannel,. For the npn nanofluidic transistor, the application of a drain voltage could cause a reverse bias in one of the two pn junctions and hence the ionic current should be saturated[12], leading to a unipolar behavior. Moreover, numerical results with negative gate voltage had non-negligible error compared to the experimental results. Therefore, the two constraints should be included in PNPS formulation to correctly describe the ambipolar behavior of the presenting partially gated IFET. The fringing fields which were generated in non-gated region to satisfy $\nabla \times \mathbf{E} = \mathbf{0}$ could modulate the whole nanochannel and hence the polarity of the entire nanochannel became positive or negative depending on the gate voltage, while the gate voltage was applied only near the center of nanochannel. Additionally, the

condensed layer formed by counter-ion in the vicinity of the highly charged oxide/electrolyte interfaces let over-modulated surface charge drop down, so that the non-negligible numerical error at larger gate voltages was resolved. Therefore, fringing field effect and counter-ion condensation were essential constraints in IFET analysis.

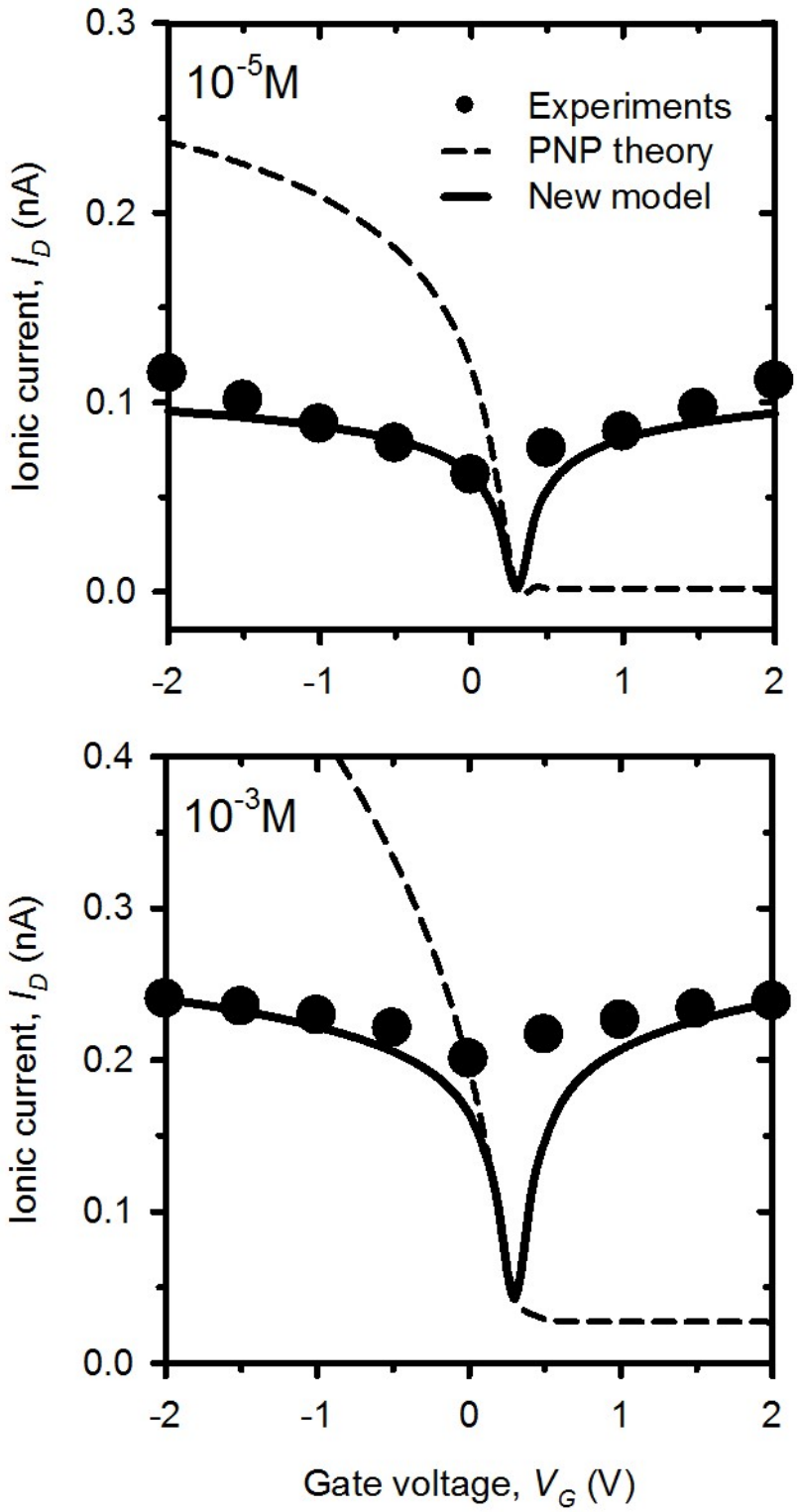

Fig 5.7 Numerical matching of PNP theory and our new model with experimental values that were measured at V_D=+2V. Bulk electrolyte concentration, c_0 was (a) 10^{-5}M and (b) 10^{-3}M.

5.3.7 Sensitive polarity inversion

The presenting IFET had the lower threshold voltage to inverse the polarity of the nanochannel than previously reported IFETs[13, 14]. We defined the threshold voltage V_{th} as required gate voltage to regulate the zero-polarity of the nanochannel. When gate voltage was higher than V_{th}, the nanochannel had the positive polarity and *vice versa*. Using the condition of σ_0=0 at V_G= V_{th}, we derived the simplified equation for V_{th} related to oxide capacitance C_{ox} and inherent surface charge density σ_0 as

$$V_{th} = -\frac{\sigma_0}{C_{ox}} \qquad \text{Eq. 5.2}$$

Equation 5.2 presented that IFET with higher oxide capacitance and lower inherent surface charge density had lower threshold voltage, leading to a fast polarity inversion. Since Al_2O_3 used in this work had near-zero surface charge density (-1.5mC/m^2) and capacitance of all-around-gate structure (5.06mF/m^2) was 5 times higher than planar-gate structure, the threshold voltages of our device were calculated to be 0.2964V from equation 5.2 and 0.2967V from numerical simulations which were superior to other IFET' s V_{th}[13, 14] as shown in Figure 5.8.

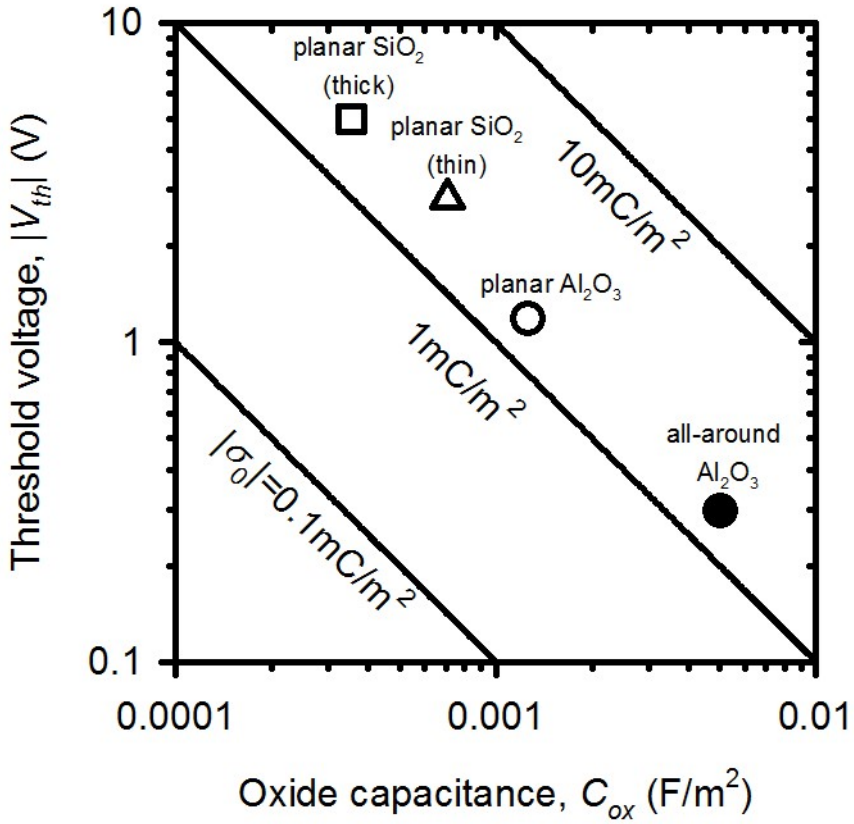

Fig 5.8 Threshold voltages of various IFET devices. Thick planar gate on SiO_2 (□) and thin planar gate on SiO_2 (△) were referred from literatures

5.4 Conclusion

In this work, we developed a transparent all-around-gated ionic field effect transistor (IFET) which has an ambipolar characteristic and can be operated at wide range of electrolyte concentrations (10^{-5}M~1M). Due to the relatively low oxide capacitance of a planar-gate structure and the inherently high surface charge density, a traditional IFET can only control the same polarity of charged species as the surface charge of nanochannel. To enable the polarity-independent control, all-around-gate structure was adapted to increase the efficiency of gate effect compared to the planar-gate structure and we used Al_2O_3 as oxide layer which has lower surface charge density than SiO_2. As a result, an ambipolar behavior was obtained by experiments and was validated by numerical simulations with a fringing field effect and a counter-ion condensation which had not been considered as major factors before. The numerical results demonstrated that the application of gate voltage can drop the electric field around the gated region so that one can possibly lower the translocation velocity of charged molecules through the nanochannel. In addition, the fabricated all-around-gated IFET had the lowest threshold voltage as required gate voltage to regulate the zero-polarity of the nanochannel. The use of this ambipolar IFET would provide significant advantages to cost-effective/on-demand/sensitive control of charged species such as ions (negative or positive), DNA (negative), RNA (negative), and

proteins (negative or positive) regardless of their polarity which is important in a biomedical analysis such as DNA sequencing through nanopore, medical diagnosis system and point-of-care system, etc.

Reference

(1) Daiguji, H.; Yang, P.; Szeri, A. J.; Majumdar, A. Nano Letters 2004, 4, 2315.

(2) Guo, W.; Cao, L.; Xia, J.; Nie, F.-Q.; Ma, W.; Xue, J.; Song, Y.; Zhu, D.; Wang, Y.; Jiang, L. Advanced Functional Materials 2010, 20, 1339.

(3) Wanunu, M.; Morrison, W.; Rabin, Y.; Grosberg, A. Y.; Meller, A. Nat Nano 2010, 5, 160.

(4) Kim, Y.; Kim, K. S.; Kounovsky, K. L.; Chang, R.; Jung, G. Y.; dePablo, J. J.; Jo, K.; Schwartz, D. C. Lab on a Chip 2011, 11, 1721.

(5) Kinnaman, T. C. Ecological Economics 2011, 70, 1243.

(6) Kim, S. J.; Ko, S. H.; Kang, K. H.; Han, J. Nat Nano 2013, 8, 609.

(7) Stein, D.; Kruithof, M.; Dekker, C. Physical Review Letters 2004, 93, 035901.

(8) Smeets, R. M. M.; Keyser, U. F.; Krapf, D.; Wu, M.-Y.; Dekker, N. H.; Dekker, C. Nano Letters 2005, 6, (1), 89-95.

(9) Reto, B. S.; Jongyoon, H.; Philippe, R. Reviews of Modern Physics 2008, 80, (3), 839.

(10) Cho, I.; Sung, G.; Kim, S. J. Nanoscale 2014, 6, (9), 4620-4626.

(11) Kim, S. J.; Wang, Y.-C.; Lee, J. H.; Jang, H.; Han, J. Physical Review Letters 2007, 99, (4), 044501.

(12) Cheng, L.-J.; Guo, L. J. ACS Nano 2009, 3, (3), 575-584.

(13) Rong, F.; Min, Y.; Rohit, K.; Arun, M.; Peidong, Y. Physical Review Letters 2005, 95, (8), 086607.

(14) Guan, W.; Fan, R.; Reed, M. A. Nat Commun 2011, 2, 506

Chapter 6. The equivalent electric circuit for nanofluidic device

6.1 Introduction

6.1.1 The response time of nanofluidic device

That research of nanofuidics has also been actively conducted in accordance with the development of Nanofluidic application described in the first chapter[1,2,3]. In point of commercialization, nanofluidic device consisting nano structure used for a part of "lab on a chip" than used alone (Fig 6.1 (a)) [4]. For example, Bio application device which detect a DNA in a blood divide few parts of function. : a part having a function of filtering the micro-sized materials, such as red blood cells, a part function of duplicating DNA for improving the detection, a part function of observing for the electrical signal etc. When the application is working by gathering parts having various function, it is important to understanding each a response time of part for grasping the overall device performance. (Fig 6.1(b))

Thus, we measured the response time of nanofluidic device. As a result, we were unable to analyze the simple sum of bulk resistor and nano structure resistor and need new electrical circuit model.

(a)

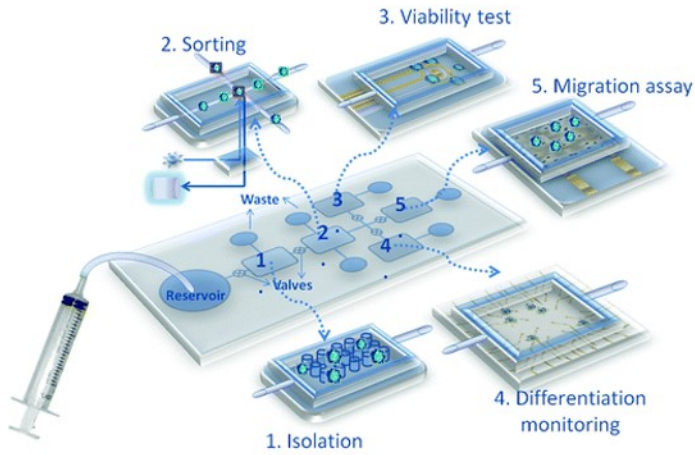

(b)

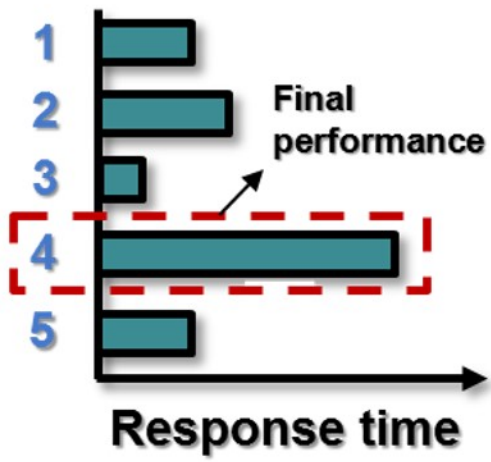

Fig 6.1 (a) the schematic picture of "Lab on a chip" (b) The response time of " Lab on a chip"

6.1.2 RC circuit delays: basic concept

Figure 6.2 (a)[5] shown the schematic RC simple circuit which resistor and capacitor are connected in series. The first moment which have applied by the voltage in this electric circuit, all of the voltage are applied to the resistor and capacitor operates as a conducting wire happening dielectric polarization. However, charge are build up to this capacitor as time goes on. Applied to the resistor voltage is dramatically reduced. Finally, all of the voltage apply to the capacitor. The current of resistor are reduced like the voltage of resistor as time goes on. In the end, current of resistor is zero. In order to compare this response time and the other device element, the "RC delay time" is defined as the time it took for maximum voltage is reduced to 1/e and it is expressed following the equation. The term of multiplied RC, τ is called the "RC time constant"[5].

$$V(t) = V(1 - exp\left(-\frac{t}{RC}\right))$$

Eq. 6.1

$$\tau = R * C$$

Eq. 6.2

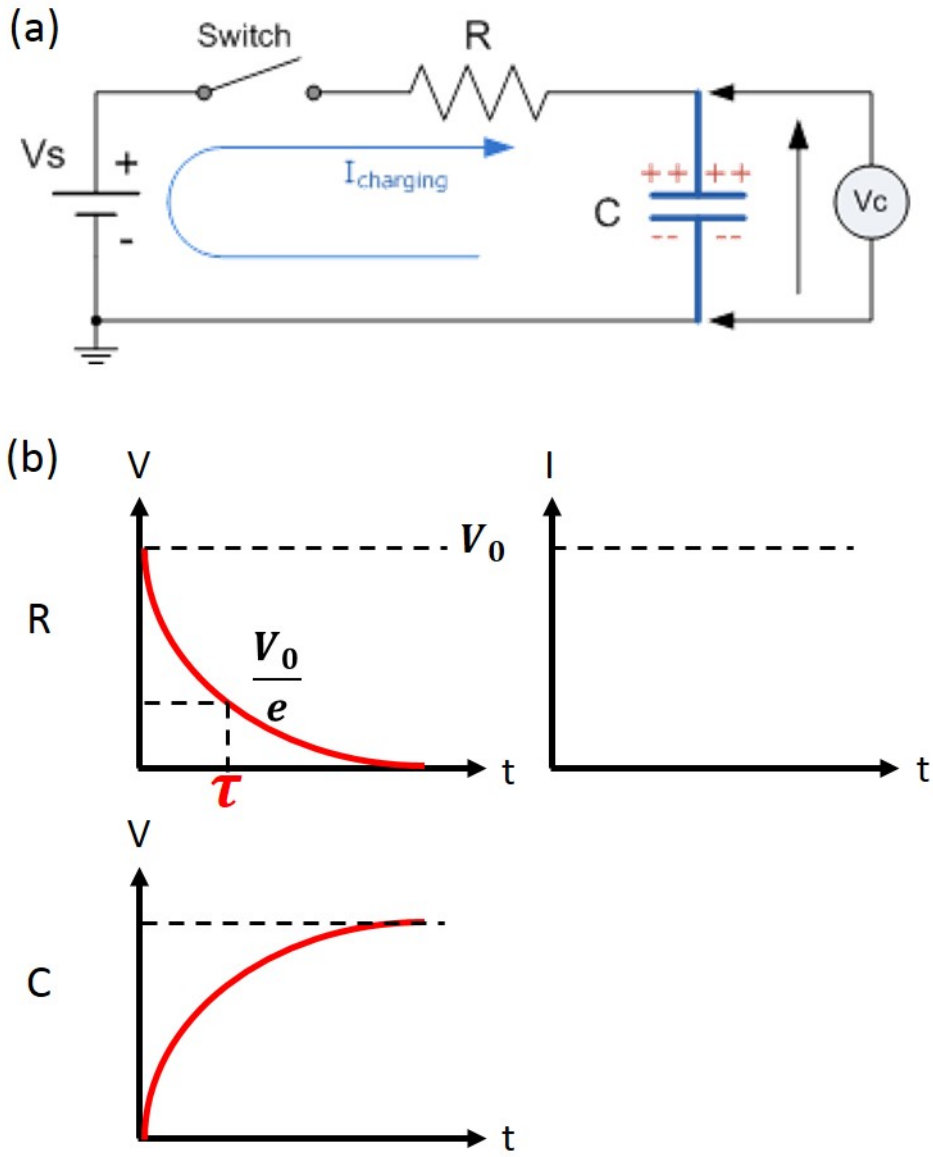

Fig 6.2 (a) The schematic figure of Simple RC circuit (b)voltage and current with time variation of resistor and capacitor.

6.2.2 Previous research: RC delay time with nanofluidic device

Smeets et. al[6] developed the new equation which analyze the response time of nanopore device. The equation 6.3 adapted the RC delay time equation of classical electromagnetic theory and adjusted to nanofluidic device.

$$i(t) = (\frac{V_\Delta}{R_C} - I_0)exp\left(\frac{-t}{R_p C_p}\right) + I_0$$

Eq. 6.3

V_Δ is applied voltage at nanopore device. R_C is the resistor of chamber, I_0 is the saturation ionic current. R_p is the resistor of nanopore. C_p is the capacitor of nanopoer membrane.

The equation 6.3[6] show that ionic current was approached the saturation ionic current I_0 when the time flows the infinitely and ionic current was determined by the resistor of chamber R_C when the time is zero, t=0. Thus, we can understand the change of ionic current from t=0 to t=∞ using this equation 6.3.

Figure 6. 3(a)[6] showed that the experiment results (black dots) and fitting line (red line) which followed by the equation 6.3 were well matched. However if the scale of figure 6.3 (a) are changed the logarithm scale, the fitting data (red line) clearly failed at upper 50

micro-sec like figure 6.3 (b)[6]. This journal mentioned that *"A fit of an ideal capacitor's response to the data is shown by the red line, which clearly fails to give a valid description for t = 50 us."* and they expressed that the effect of dielectric loss was the reason why the fitting data was failed above 50 micro-sec region. However they were unable to define exactly what "the effect of dielectric loss" is and rewrite a correct equation included "the effect of dielectric loss".

In this chapter, we were developed a new model which more clearly explain the response time of nanofluidic device. We focused that Smeets' equation considered the resistor of chamber R_C , the capacitor of nanopore membrane C_p and the resistor of nanopore R_p. However nanopore system also have the charge polarization region (Electric double layer) which was generated by gathering of counter ions. So we needed to consider the affection of EDL as a new capacitor of nanopore system for analyzing the response time.

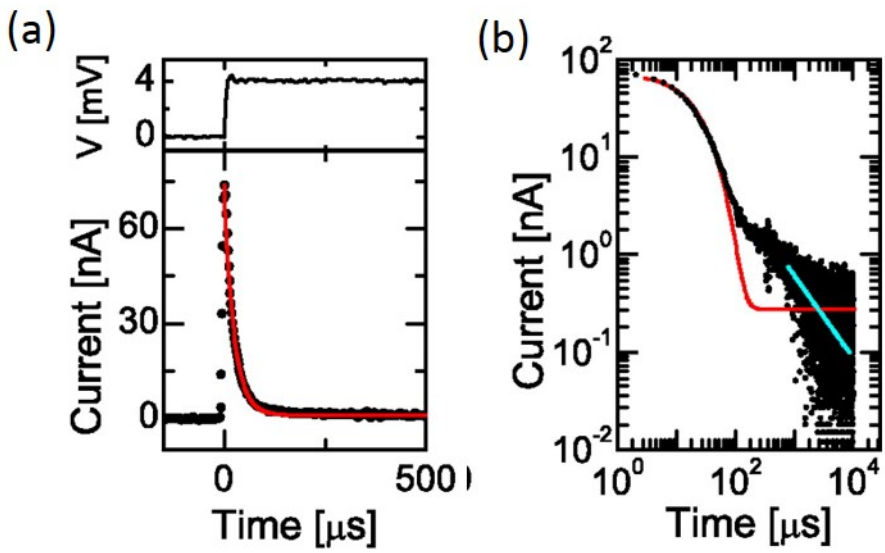

Fig 6.3 The ionic current – time graphs of nanopore device (a) linear scale. the experiment results (black dots) and fitting line (red line) which followed by the equation 6.3 were well matched. (b)logarithm scale. the fitting data (red line) clearly failed at upper 50 micro-sec.

6.2 Materials & methods

Si based nanpore device fabrication was well established.[7-9] This report was followed them. 500um Silicon wafer were coated back and forth with 100nm silicon nitride (Si3N4) using a low pressure chemical vapor deposition (LPCVD) (Figure 6.4 (a)). For opening a window in the back side of wafer, photolithography and reactive ion etching (RIE) were used to remove the micro scale of SiN layer (Figure 6.4 (b)), after which a KOH wet etch removed the 500um silicon (Figure 6.4 (c)). This KOH wet etching condition is 78degree at 10hours. Silicon wet etch rate is 5um/hr at this condition and because etch slop is followed Si (111) plane after 10hours, final free standing silicon nitride membrane size was micro scale (Figure 6.4 (d)). We employed focused ion beam to fabricate 100 nm diameter nanopore (FIB)(Figure 6.4 (e)) and atomic layer deposition (ALD) to reduce the size of the nanopore with tunable and controllable diameter in a silicon nitride membrane (Figure 6.4 (f)).

Prior to measurement of ionic current through nanopre, the silicon nitride membrane was treated by oxygen plasma about 1min to enhance the hydrophilicity of nanopore surface.

The silicon nitride membrane was placed between two components of flow cell. One component was consisted of Teflon jig which functions as a fluidic channel and the other was a

polydimethylsiloxane (PDMS) block which function as adhesion and sealing layer. And Ag/AgCl electrodes were immersed at both fluidic channels and connected to an amplifier (AXON patch 200B, Axon instruments, USA) (Figure 6.5)

The ionic current was measured two different voltage region using a potassium chloride (KCl) buffer solution at pH7 in the concentration range from 10-5M to 1M. The high voltage region started from 100mV to 500mV at 100mV step. And the low voltage region increased 2mV to 6mV at 2mV step. The ionic current of the highest point beyond 200nA was cut off due to the equipment limitation of Axon patch clamp. So the experiment results of high voltage only used confirm data

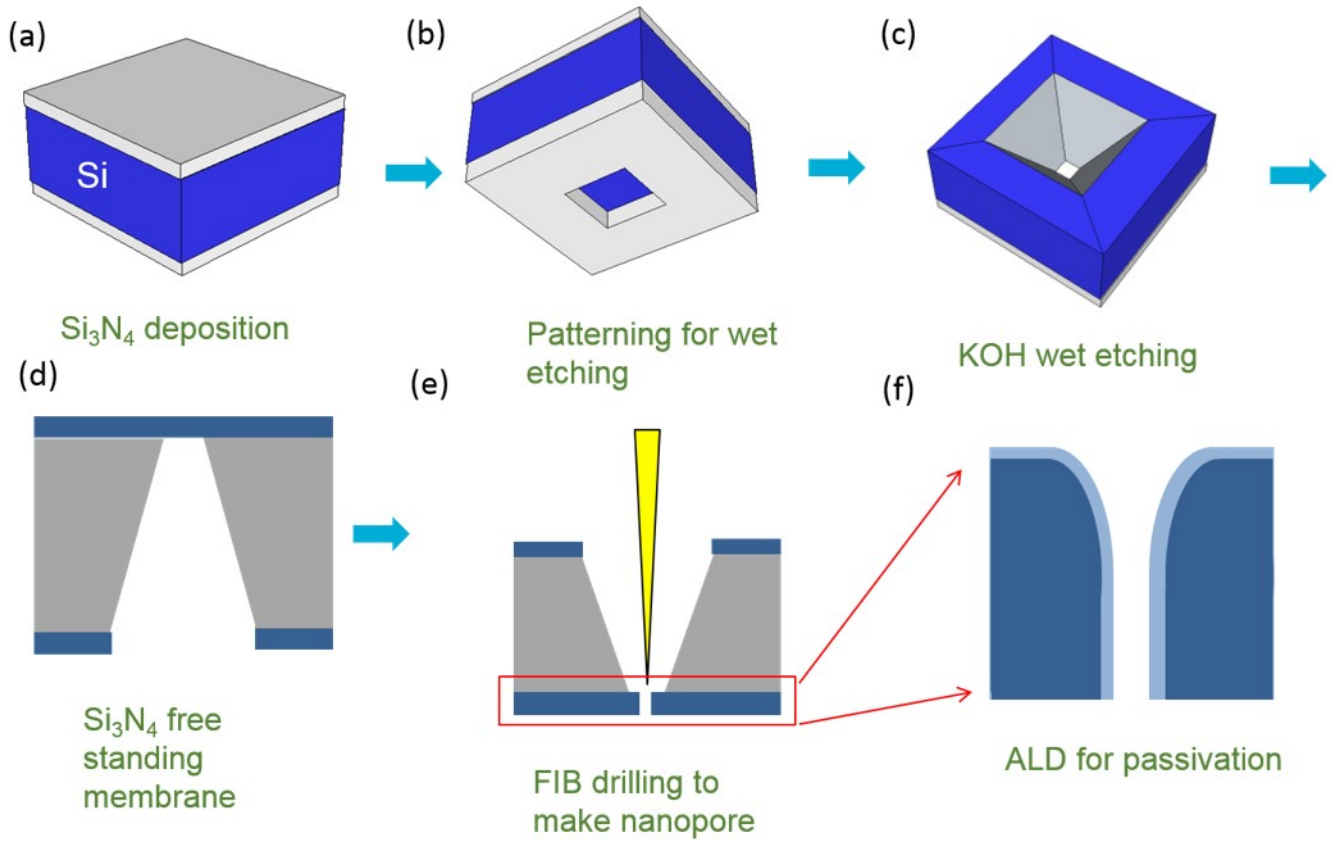

Fig 6.4 Schematics of fabrication process.

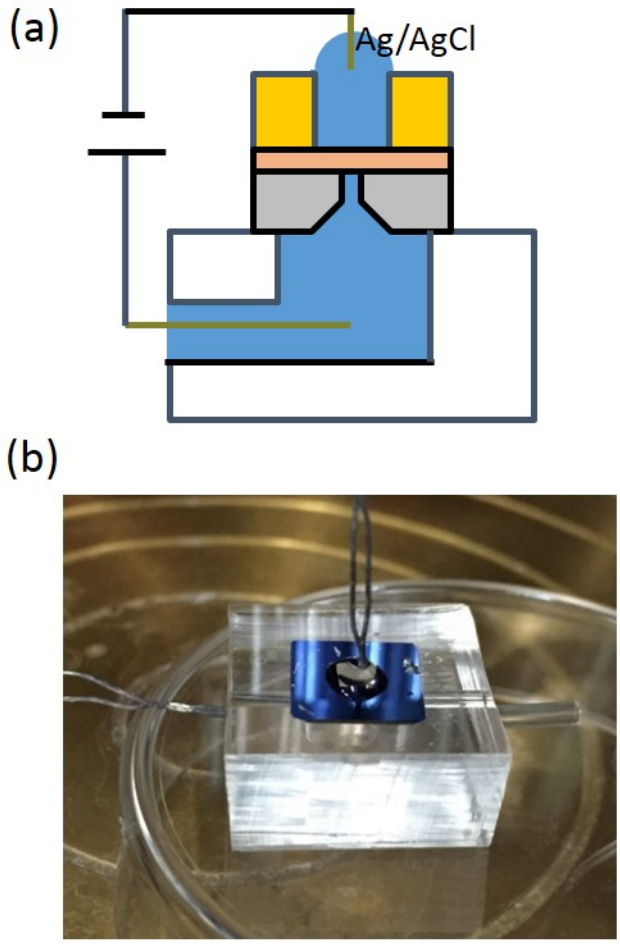

Fig 6.5 (a) The schematic figure of electric circuit of nanopore measurement (b) photograph of measurement setup

6.3 Results and discussion

6.3.1 The new electric circuit model for analyzing the response time

The Figure 6.6 shown the electric circuit of Figure 6.6 (a) Smeets' model and Figure 6.6 (b) our model. The difference between of them is the capacitor C_{EDL} which was generated by electric double layer inside the nanopore. Ionic current equation as time was developed for modeling the Figure 6.6 (b) which include the capacitor C_{EDL}.

Our model (Figure 6.6 (b)) have five parameter which are 3 resistor and 2 capacitor. Therefore we need five equations due to determine the five parameter. First, we made the five equation followed by Kirchhoff' law.

$$I_1 = \frac{V_1 - V_2}{R_1} \qquad \text{Eq. 6.4}$$

$$I_2 = \frac{V_2 - V_3}{R_2} \qquad \text{Eq. 6.5}$$

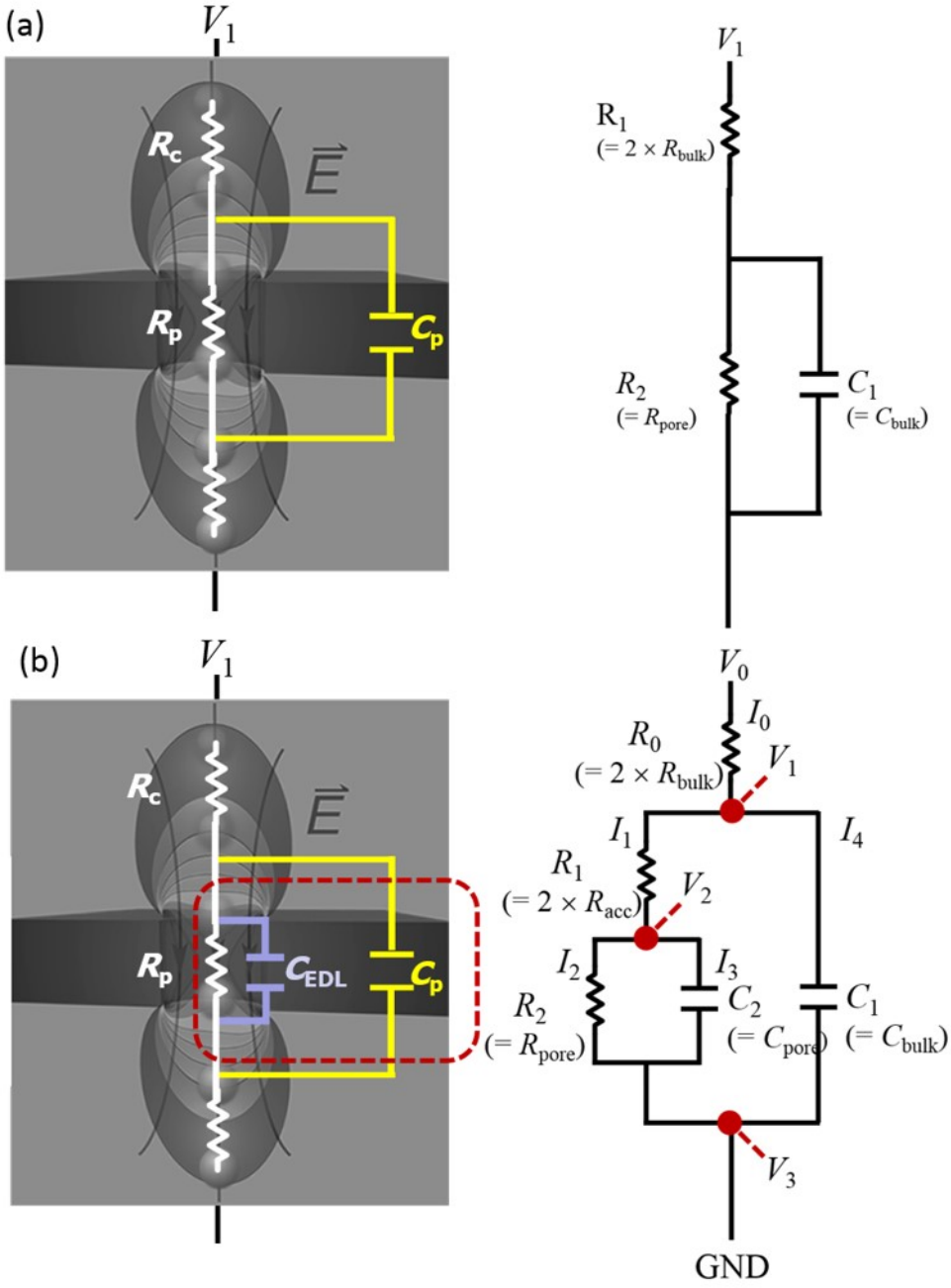

Fig 6.6 The schematic figure and electric circuit of (a) Smeet' model (b) our new model.

$$I_3 = \frac{V_3}{R_3}$$ Eq. 6.6

$$I_4 = C_2 \frac{V_3}{t}$$ Eq. 6.7

$$\mathrm{I_5} = C_1 \frac{\mathrm{V_2}}{\mathrm{t}}$$ Eq. 6.8

We have a simultaneous second differential equation (Eq. 6.9) using the equations 6.4 ~6.8.

$$\mathrm{R_1C_1R_2C_2}\frac{\mathrm{d^2V_2}}{\mathrm{dt^2}} + \left[\left(1+\frac{\mathrm{R_1}}{\mathrm{R_2}}\right)\mathrm{R_1C_1} + \left(1+\frac{\mathrm{R_2}}{\mathrm{R_3}}\right)\mathrm{R_2C_3}\right]\frac{\mathrm{dV_2}}{\mathrm{dt}} + \frac{(\mathrm{R_1}+\mathrm{R_2}+\mathrm{R_3})\mathrm{V_3}}{\mathrm{R_2}} = \mathrm{V_1}$$

Eq. 6.9

and the equation 6.9 can solve using the general solution. So, we can get the final equation 6. 10.

$$\mathrm{I(t)} = \mathrm{I_{sat}} + \mathrm{Aexp}\left(-\frac{\mathrm{t}}{\tau_+}\right) + \mathrm{Bexp}\left(-\frac{\mathrm{t}}{\tau_-}\right)$$ Eq. 6. 10

$$\tau_{\pm} = \frac{1}{C_1 C_2}\left[-\frac{\beta}{2}C_1 - \frac{\alpha}{2}C_2 \pm \sqrt{\left(\frac{\beta}{2}C_1 - \frac{\alpha}{2}C_2\right)^2 + \frac{C_1 C_2}{R_2^2}}\ \right]$$

Eq. 6. 10.1

$$\alpha = \frac{1}{R_1} + \frac{1}{R_2}$$

Eq. 6. 10. 2

$$\beta = \frac{1}{R_2} + \frac{1}{R_3}$$

Eq. 6. 10. 3

The equations 6.10.1~6.10.3 is the detail explanations of equation 6. 10.

6.3.2 Comparison new model with Smeets' equation

The difference of smeets' model and our model is the presence or absence of the EDL capacitor in electric circuit. The difference was able to express the flowing simple equations.

$$I(t) = I_{sat} + Aexp(-\frac{t}{\tau})$$

Eq. 6.11

$$I(t) = I_{sat} + A'exp(-\frac{t}{\tau_+}) + B'exp(-\frac{t}{\tau_-})$$

Eq. 6.12

A, A' and B' are constant value in the same system. $\tau = R_2 * C_1$

τ_+, τ_- are followed Eq. 6. 10. 2 and Eq. 6. 10. 3. The equation 6.11 is the simplified Smeets' equation and the equation 6.12 is the simplified our equation. Our equation have one more exponential term which is generated by the EDL capacitor.

The figure 6.7 shown the experimental data of nanopore device in logarithm scale. The black dots are experimental ionic current as time goes on. The blue line is followed Smeets' model and the red line is followed our model. This graph obviously was announced that

our model have a good fitting value than Smeets model. Two capacitors were calculated with the equation 6. 10 and it was displayed on the figure 6.8. This figure notified below facts that First, the bulk capacitor which was generated by nanopore membrane was independent the concentration of solution. Second, pore capacitance was changed by the concentration of solution. Pore capacitance have the constant value until 10^{-2}M. In above concentration, pore capacitance was increased 10 fold in proportion with concentration.

We can some careful estimations. The capacitor of nanopore membrane which was made by SiN layer should be the constant value because of native capacitor are independent of concentration. However our new capacitor, nanopore capacitor which was affected by the electric double layer should be sensible with the change of concentration and divided two region like ionic conductance (Figure 5.2). We think that even through the pore capacitor is smaller 1000 times than nanopore membranes, it is enough to change the response time of nanopore system because of the huge nanopore resistor.

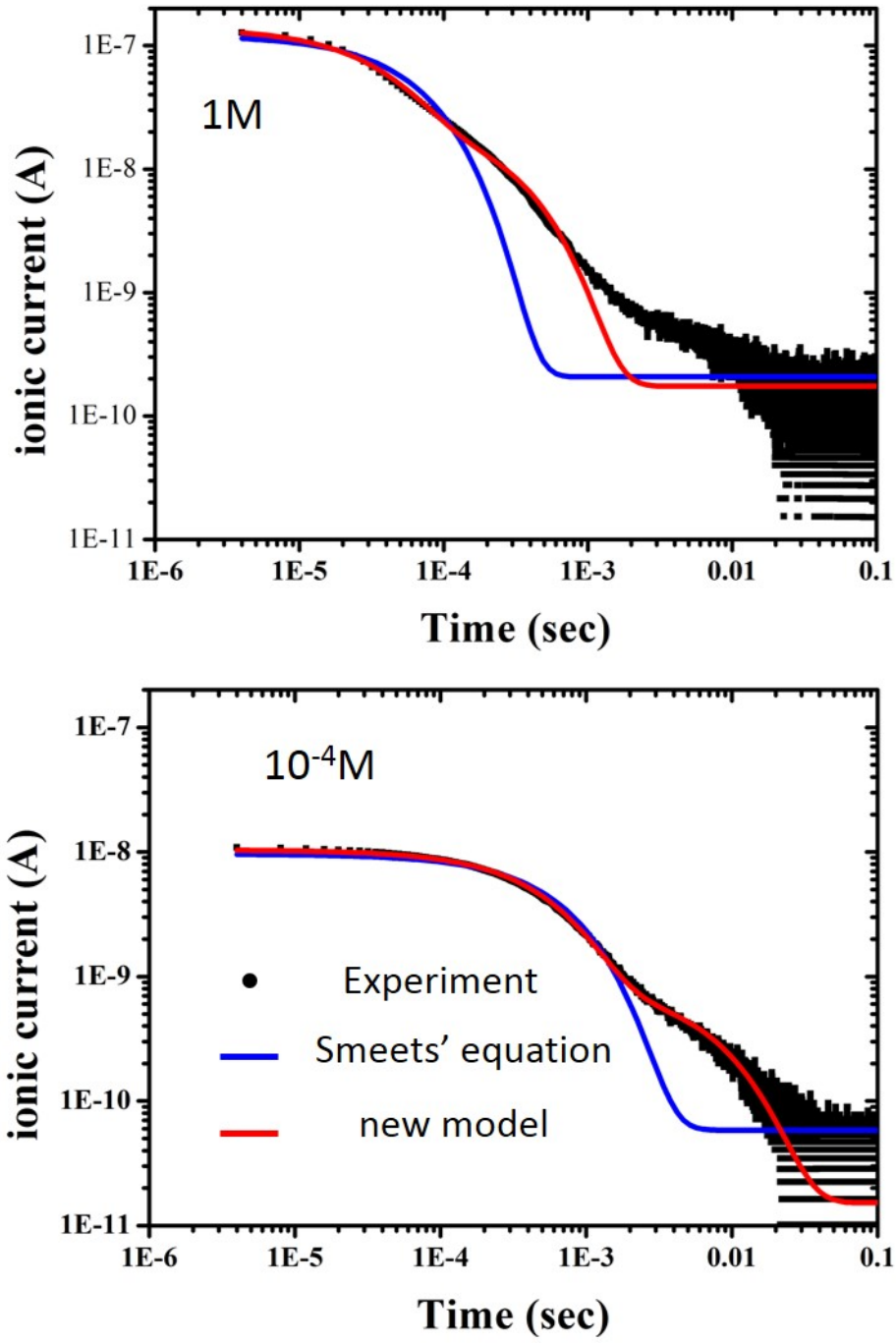

Fig 6.7 The ionic current – time graph with nanpore system (a) 1M KCL (b) 10^{-4}M KCL by logarithm scale.

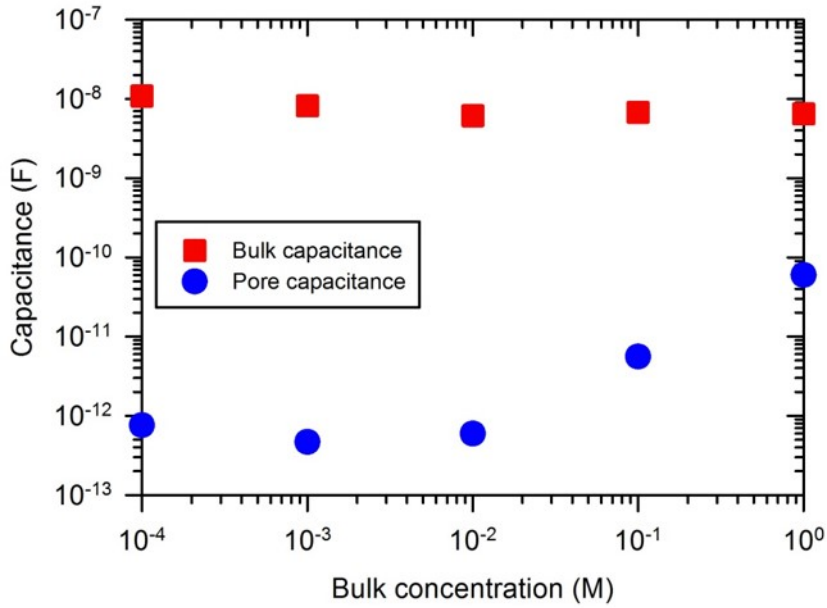

Fig 6.8 Capacitance – bulk concentration graph.

6.4 Conclusion

The ambipolar IFET showed slow response time during ionic current measurement. Smeets analyzed the slow response time using a simple RC electric circuit, but it does not fit well to experiment data below t = 50 us. We hypothesized that the long response time comes from the electric double layer capacitor. Thus we developed a new model and equation that includes "EDL capacitor". Silicon nitride nanopore device was made by traditional fabrication method. The device measurement was done by patch clamp. By matching the new model to experimental data, we showed the possibility of a better theory than Smeets' equation.

References

(1) Utkur, M. et.al, Nanotechnology, 21, 395501 (2010).

(2) Wanunu, M.; Meller, A. Nano Letters, 7, 1580 (2007).

(3) Fan, R. et. al, Nat. Mater., 7, 303-307 (2008)

(4) E. Primiceri et al., Lab on a Chip, 13, 3789 (2013)

(5) http://www.electronics-tutorials.ws

(6) R.M.M.Smeets et.al, PNAS, 105, 417 (2008)

(7) A. Singer *et al. Nano Lett. 10*, 738 (2010)

(8) R. M. M. Smeets *et al. Nano Lett. 6*, 89 (2006)

(9) G. F. Schneider *et al. Nano Lett. 10*, 3163 (2010)

Chapter. 7 Conclusion

7.1 conclusion

In this dissertation, the advanced device was developed for overcoming the limitation of IFET which can be manipulate charged species pass through nanochannel. And the slow response time of nanofuidic device was studied for improving the device.

Traditional IFETs have the unipolar behavior and low gate efficiency. In order to overcome these limitations, Al_2O_3 which has near-zero surface charge density was used for IFETs to have the ambipolar behavior and all around gate structure was developed to enhance the gate efficiency. All around gated ambipolar ionic field effect transistor was fabricated with electron beam lithography and atomic layer deposition. The ionic current of the IFET was measured at various gate voltages (-2V ~ +2V). As a result, our device showed ambipolar behavior unlike traditional IFETs which have unipolar behavior. Our experimental data were theoretically matched with the new model (fringing effect, ion condensation). Finally, our device demonstrated higher gate efficiency than those of traditional IFETs.

The ambipolar IFET showed slow response time during ionic current measurement. Smeets analyzed the slow response time using a simple RC electric circuit, but it does not fit well to experiment data below t = 50 us. We hypothesized that the long response time comes from the electric double layer capacitor. Thus we developed a new

model and equation that includes “EDL capacitor”. Silicon nitride nanopore device was made by traditional fabrication method. The device measurement was done by patch clamp. By matching the new model to experimental data, we showed the possibility of a better theory than Smeets’ equation.

Abstract (in Korean)

이 박사학위논문에서는 나노구조체 사이를 흐르는 전하를 가진 물질을 제어할 수 있는 능동소자인 IFET 의 현상을 이해하고, 그 한계성을 극복하여 개선된 소자를 개발하였다. 또한 나노플루이딕 소자가 가진 한계성이 낮은 응답속도에 대한 연구를 진행하였다.

우리는 넓은 농도범위(10^{-5}M~1M)에서 사용가능하고 나노채널 사이를 지나가는 물질을 극성에 상관없이 조절할 수 있는 all-around type의 전기장 구동 이온 트랜지스터를 개발 하였다. 이 전기장 구동 이온트랜지스터(IFET)는 나노채널 부분을 원통형으로 게이트 전극이 모두 감싸고 있으며, 거의 0에 가까운 표면전하량을 가진 알루미늄 옥사이드(Al_2O_3)로 게이트 옥사이드(gate oxide)를 사용하였다. 이 소자를 실험적으로 그리고 이론적으로 특성을 평가하였다. 그 결과, 우리는 모든 극성에서 조절 가능한 특성이 거의 0에 가까운 표면전하량을 가진 알루미늄 옥사이드로부터 오고, all around gate type으로 만들 경우 기존의 평판 게이트 구조 보다 5배이상의 게이트 효율성이 올라감을 알게 되었다. 우리의 이론계산은 기존에 연구된 Poisson-Nernst-Plank-Stokes (PNPS) 이론을 받아들이고 여기에 fringing field effect와 counter-ion condensation 을 고려하여 새로운 모델을 만들었다. 그 결과, 실험값과 이론값이 잘 맞는다는 사실을 알게 되었다. 이 소자는 세일가스을 개발할 때 사용된 높은 농도의 물(1M)에서도 사용될 수 있다. 게다가, 기존에 개발된 IFET는 게이트 옥사이드의 표면전하량에 의해서 실제로 조절할 수 있는 물질이 정해져 게이트 옥사이드와 다른 극성을 가진 물질은 조절할 수 없었던 것과는 달리 우리가 개발한 소자는 서로 다른 극성을 가진 물질을 모두 조절할 수 있는 장점을 가진다. 이는 특히, DNA시퀜싱 이나

의학 진단시스템 개인의료 시스템에서 매우 중요한 점으로 사용될 것이다.

그러나 이렇게 개발된 ambipolar IFET는 이온 전류를 측정하는 과정에서 매우 늦은 반응속도를 보인다. 이를 Smeets는 간단한 RC 전기회로를 통해 해석하고자 하였으나, 실험결과 50us 이상에서는 이론과 실험값이 잘 맞지 않았다. 이에 우리는 늦은 반응속도가 전기이중층에 의해서 발생할 것이라고 가정하고, EDL 캐패시터를 포함한 새로운 모델을 개발하였다. 우리는 실리콘 나이트라이드 (SiN)로 나노포어를 만들어 실험하고 새로운 모델과 비교하였다. 그 결과 Smeets의 모델보다 더 잘 맞는다는 사실을 보일 수 있었다.

List of publications

Paper

1. NANOSCLE 7, 936 (2015) COVER LETTER

“Sub-10nm transparent all-around-gated ambipolar ionic field effect transistor” 1저자

2. Nano Letters 10, 3324 (2010)

“Sub-10-nm Nanochannels by Self-Sealing and Self-Limiting Atomic Layer Deposition” (3저자)

3. Electrochem. Solid-State Lett 13(2), K8, 19 2010 (2010)

“Selective incorporation of colloidal nanocrystals in nanopatterned SiO2 layer for nanocrystal memory device” (4저자)

4. Thin Solid Film 518, S217, 21, 1 Jan (2010)

“Controlling dislocation positions in silicon germanium (SiGe) buffer layers by local oxidation”(4저자)

5. Journal of Crystal Growth, 311, 1539-1544 (2009)

“Behavior of ultraviolet emission from nanocrystalline embedded ZnO film synthesized by solution-based route “ (2저자)

Patent

제한된 영역을 가지는 나노 채널 구조를 이용한 이온 소자 (Ion device using nano-channel having notched structure) **등록번호** : 10-1432558 , **등록일** : 2014-08-14